3-2022

Optimization of a Multi-Layered Target for a Pulsed Power Neutron Source

Zachary D. Bretz

Optimization of a Multi-Layered Target for a Pulsed Power Neutron Source

THESIS

Zachary D. Bretz, Civilian

AFIT-ENP-MS-22-M-080

DEPARTMENT OF THE AIR FORCE
AIR UNIVERSITY

AIR FORCE INSTITUTE OF TECHNOLOGY

Wright-Patterson Air Force Base, Ohio

AFIT-ENP-MS-22-M-080

Optimization of a Multi-Layered Target for a Pulsed Power Neutron Source

THESIS

Presented to the Faculty

Department of Engineering Physics

Graduate School of Engineering and Management

Air Force Institute of Technology

Air University

Air Education and Training Command

in Partial Fulfillment of the Requirements for the

Degree of Master of Science

Zachary D. Bretz, B.S.M.E

Civilian

March 2022

AFIT-ENP-MS-22-M-080

Optimization of a Multi-Layered Target for a Pulsed Power Neutron Source

THESIS

Zachary D. Bretz, B.S.M.E
Civilian

Committee Membership:

Dr. Juan J. Manfredi
Chair

Maj James E. Bevins, Ph.D.
Member

Dr. Darren E. Holland
Member

Dr. Paul E. Adamson
Member

Abstract

The ability to create neutron environments is critical fora wide variety of applications including national security, materials science, and medical research. It is also helpful in medical, material, and other research. The U.S. Naval Research Laboratory (NRL), Washington, DC, is interested in leveraging their pulsed-power facilities to produce an in-house, relatively inexpensive neutron source. NRL's facilities produce 2 MeV (from Gamble II) and 5 MeV (from Mercury) protons and deuterons. This research explored combinations of target materials to produce the most neutrons in the forward direction. Models of the reactions involved were first validated against literature experiments, then target designs were optimized with Dakota, a robust software suite used for various aspects of design exploration. The nuclear reactions and targets were modeled with MCNP, a Monte Carlo neutral particle transport code. A code base for scaling and future design work was also developed. The materials used in the optimization were lithium, beryllium, carbon, and deuterated polyethylene (CD_2).

The validation revealed discrepancies between the cross section libraries and literature. The CP2020 and JENDL/DEU libraries performed relatively well. The TENDL-2019 library greatly underperformed for the deuteron reactions. The ENDF/B-VIII.0 library also deviated in some cases from the existing data.

The optimizations resulted in four unique targets, but came with a large amount of uncertainty. Lithium was shown to be the better target for the proton reactions, while beryllium was better for deuteron reactions. There were some variations of beryllium-lithium combination targets that produced the most neutrons, but these need further investigation. The carbon and CD_2 were found to produce neutrons at a much lower rate than beryllium or lithium and were not used in any target.

Table of Contents

Page

List of Figures

List of Tables

Listings

Optimization of a Multi-Layered Target for

a Pulsed Power Neutron Source

I. Introduction

1.1 Motivation

On July 18, 1945, the first nuclear device detonation occurred in the deserts of New Mexico, ushering in the atomic age [1]. The Manhattan project's culmination of the Trinity Test led to the dropping of Little Boy and Fat Man on Nagasaki and Hiroshima in an effort to end the War in the Pacific. Post-war grappling for power resulted in the first Soviet test in 1949. The Cold War culminated in tens of thousands of weapons stockpiled between the United States and Soviet Union. Today, eight countries have officially declared possession of nuclear weapons [2]. In the early 1990s, the Comprehensive Test Ban Treaty (CTBT) was developed to curb the increasing fallout associated with both nuclear testing and political tensions. Though 180 countries have signed the CTBT, it remains stagnant as several signatories, including the U.S., have yet to ratify it. Nonetheless, most countries have ceased nuclear testing, instead relying on previous tests and modeling.

Since testing has ceased, gaining a deeper understanding of nuclear weapon effects is a continued pursuit for countries to maintain viability and deterrence. As proliferation risks increase, there is greater need for testing in these environments [3]. One of the most critical and unique effects of nuclear detonations is from radiation, including x-rays, gamma rays, electromagnetic fields, and neutrons. Neutrons compose a small percentage of the total energy of a nuclear blast, and many are reduced in energy in

the debris and surrounding air [4]. Nonetheless, a sufficient number of high energy neutrons can escape and pose a serious threat to people, structures, and electronic devices at considerable distances [4]. Nuclearradiation can ionize parts of cells in the body, disrupting or altering function and potentially creating poisons. Neutrons travel great distances, passing through and radiating materials in buildings and the ground. Electronics can be irrevocably altered by neutrons, rendering them incapable of performing their original functions.

Beyond national security concerns, neutron environments are useful for other areas of research, including but not limited to physics, materials, and medicine [5–7]. Neutrons are used to probe the smallest building blocks of the universe [8]. Isotope production with neutrons expands the understanding of nuclear reactions while also creating isotopes that have a variety of useful purposes. [9]. As early as 1938, neutrons have been used in cancer therapy [10], with more progress continuing to today in fields like boron neutron-capture therapy [11–14].

The U.S. Naval Research Laboratory (NRL) in Washington, D.C. is interested in leveraging their pulsed-power capabilities to develop a neutron source for national security applications. Currently, these pulsed-power generators – Gamble II and Mercury – produce intense pulses of electrons or ions over a short period of tens of nanoseconds [15, 16]. Expanding the capability to include intense, tailored-spectra neutron beams would close gaps in current neutron testing facilities and is of interest to NRL and others in the nuclear weapons effects community in the Departments of Energy (DOE) and Defense (DOD) [3].

1.2 Background

Neutrons are produced from a variety of reactions. Nuclear fusion, nuclear fission, Brehmsstrallung photoneutrons, nuclear decays, or charged particle interactions all

produce neutrons with different energy spectra [17]. James Chadwick is credited with the discovery of the neutron in 1932 [18] via the reaction

$$\alpha + {}^{9}Be \longrightarrow n + {}^{12}C, \tag{1.1}$$

an α-particle (from the natural decay of polonium) bombarding beryllium-9 to produce carbon-12 and a neutron. (The theory of nuclear reactions will be discussed further in Chapter 2.) This type of reaction requires only a combination of a radioactive material and target. These (α,n) sources are common for producing a constant, known neutron spectra for use in laboratory or industrial settings [19]. One example is the AmBe source, which utilizes the same α-beryllium reaction as Chadwick. With a half-life of 432.6 years, ^{241}Am alpha decays, to initiate the α+^{9}Be reaction. Photoneutron sources act in a similar way, except that a γ-ray that bombards a nucleus, such as ^{9}Be, producing a neutron and other products, like ^{8}Be [20].

Fusion and fission sources are of particular interest to national security concerns. Neutrons from fusion can be produced in a facility like Lawrence Livermore National Laboratory's (LLNL) National Ignition Facility (NIF). A high-energy laser is focused on a small amount of deuterium and tritium, heating the target to several million degrees until fusion occurs, creating alpha particles and neutrons [21]. A variety of scientific facilities exist to study the neutron radiation produced by nuclear fission. One example is Oak Ridge National Laboratory's High Flux Isotope Reactor (HFIR). The design of this facility allows for a wide range of neutron energies and flux. It consists of two concentric rings of highly enriched ^{235}U fuel, allowing for an "island" in the center for high flux applications. Various moderating materials are positioned on the outside of the fuel, and several cavities allow for differing neutron energies and fluxes [22]

Accelerators can also be used to produce neutrons by bombarding ions onto certain

targets. One example of this is the 88-Inch Cyclotron at Lawrence Berkeley National Laboratory (LBNL). The cyclotron uses a combination of a static magnetic field and oscillating electric fields to accelerate deuterons to the desired energy, up to 65 MeV [23, 24]. These ions then bombard the target, inducing nuclear reactions. Neutrons and other product are produced according to the probability of the reaction, quantified by the cross section.

Indiana University also has an accelerator-based neutron source: the Low Energy Neutron Source (LENS) [25]. A linear accelerator (LINAC) delivers 7 or 13 MeV protons to a water-cooled beryllium target. Beryllium "was chosen because of its high neutron yield, high melting point, and mechanical strength" [25]. The time period of this pulse is adjustable on the order of milli- to micro seconds. The proton bombardment produces neutrons which are moderated down to the thermal range by a combination of materials, including water (which also acts as a coolant) and methane. The neutron yield is on the order of 10^{-2} neutrons per proton [25].

Spallation sources, like Oak Ridge's Spallation Neutron source (SNS) facility, also produce neutrons with charged particles like the Cyclotron and LENS but the ions are typically at much higher energies (up to the GeV range). When these high energy ions impinge upon a heavy target, a reaction called spallation occurs which results in the production of energetic neutrons [26].

The U.S. Naval Research Laboratory, Washington D.C. (NRL) has pulsed power facilities that can be leveraged to produce intense pulses of neutrons. In its most simplest form, pulsed power works by quickly releasing a large amount of power (TW range) in the form of a short (50 ns) electric pulse across an anode-cathode gap, ionizing the gas or other material which travels in the same direction as the current. This general setup can be configured to produce a variety of outputs, including electrons, x-rays, and ion beams with beam energies up to 2 MeV (Gamble II) and 5 MeV (Mer-

cury). These outputs can then impinge on a variety of targets, which then produce alternate outputs, depending on need. The focus here will be hydrogen ions in the form of protons and deuterons impinging on a target to produce neutrons [27].

1.3 Problem

This thesis will address the design of a target to maximize neutron flux from reactions using the 2 and 5 MeV proton and deuteron ions from Gamble II and Mercury, respectively. Though these facilities produce ion beams with energy spectra up to the maximum energies, for this initial study the beams will be considered monoenergetic beams are considered. The design will be conducted using a combination of optimization methods and Monte Carlo radiation transport simulations. In order to leverage the various reaction characteristics of different target materials, multiple layers of varying thicknesses will be investigated. To ensure the simulations are accurate, the neutron production reactions from multiple evaluated nuclear data libraries for each material will be validated against existing literature experimental measurements.

1.3.1 Research Objectives

The end goal is to determine from a set of materials the best target composition that will result in the highest neutron production for a given incident ion beam. Since NRL's pulsed power generators can produce both protons and deuterons, four mono-energetic incident beams will be investigated: 2 MeV protons, 5 MeV protons, 2 MeV deuterons, and 5 MeV deuterons. The 2 MeV ions will be assumed to have currents of 300 kA from Gamble II, and 60 kA for the 5 MeV ions from Mercury. The code suite will be developed in order to maximize flexibility for future studies on other parameters such as other beam profiles (particularly using ion with an energy spectrum rather than a single energy) and additional materials.

The approach to reaching this goal will begin with modeling individual reactions in MCNP [28] to validate the cross section libraries against existing literature. The reactions will cover a range of incident particle energies, comparing the outgoing neutron spectra and total production to the literature. Then, the optimization will be performed with Sandia National Laboratory's (SNL) Dakota software [29]. Dakota will loop through different combinations of target layer materials and thicknesses, performing MCNP simulations for each to converge on the best solution.

The specific outcomes for this research are:

- Validating models (specifically using the cross section libraries) of neutron-producing reactions at energies below 8 MeV;
- Optimized targets for
  - 2 MeV protons,
  - 2 MeV deuterons,
  - 5 MeV protons, and
  - 5 MeV deuterons;
- Code suite of MCNP, Dakota, and supporting files written with design scaling in mind.

1.3.2 Assumptions and Limitations

This research will be limited to the following reactions: Li(p,n), Be(p,n), D(d,n), Li(d,n), Be(d,n), and C(d,n). These are several of the most common reactions in literature for neutron production [25, 27, 30, 31]. While there may be other materials that may result in higher neutron yields (like tritium), they were not considered in this work and are left for future study. The results are limited to accuracy of the

cross-section libraries that are the basis of MCNP. When performing the validation, the difference between the simulation results and the literature must be noted.

The extent of this research will be limited to the neutron production from the (p,n) or (d,n) reactions in MCNP simulations. Additional products from reactions of protons or deuterons on the target materials, such as gammas, are not tracked. This means secondary reactions – such as deuterons reacting with tritium produced by D-D fusion – will be left out. These secondary reactions may increase neutron production and change outgoing neutron energy spectra, but assessment of these effects are beyond the scope of this research. It is recommended that this is explored further when realistic energy spectra of proton and deuteron beams are implemented.

Finally, this research will not go into engineering target design: how the target is made, what holds it, how it thermo-mechanically responds, if it needs cooling, what shielding is needed, etc.

II. Theory

This chapter provides the theoretical background for the neutron-producing reactions discussed in the rest of this thesis. A high-level view of both proton- and deuteron-induced neutron production will be discussed. In addition, the basis for the Monte Carlo modeling approach in MCNP will be introduced as well as a surface-level look at optimization methods will be discussed.

2.1 Nuclear Reactions

Nuclear reactions can be represented in the form

$$\mathrm{a} + \mathrm{X} \longrightarrow \mathrm{Y} + \mathrm{b}, \tag{2.1}$$

where a is the incident particle, X is the target nucleus, Y is a heavy product which usually remains contained in the bulk material, and b is a lighter product that exits the bulk material and can be measured. The generally accepted shorthand for this reaction is X(a,b)Y and the reaction type is referred to as (a,b). In the present case, the incident particle a is a projectile accelerated at the target nucleus X, which is usually the larger particle in a bulk material matrix and stationary in the laboratory frame.

Specific nuclear reaction mechanisms vary depending on the reactants, products, kinetic energies, and the distance between the target and projectile as characterized by the impact parameter. The two extremes are given by compound nuclear reactions and direct reactions. There are also scattering reactions, where a and b are the same particle. These can be elastic – where the target nucleus remains in the ground state or inelastic – where some energy is imparted to the target nucleus, leaving it in an excited state.

2.1.1 Proton Reactions

Compound reactions occur when the incident particle's energy (E_i) is contained within the target nucleus and shared by the nuclei, creating an intermediate, excited combined state. This reactions takes the form

$$a + X \longrightarrow C^* \longrightarrow Y + b, \tag{2.2}$$

where C^* is the excited compound state. When the impact parameter is small compared to the target radius, the incident particle is more likely to collide with and impart energy to the inner target nucleons, increasing likelihood of creating a compound nucleus. Through successive scatters by the initial particle and other nucleons, the initial energy is distributed over many nucleons. This resulting combined system of incident particle and target nucleus, called the compound nucleus, is a new isotope in an excited state. Like molecules evaporating from a hot liquid [20], nucleons can be emitted by the decay of this intermediate state. The higher the energy of the excited nucleus, the higher the probability of nucleon escape. Compound nucleus formation and subsequent decay happens on the order of 10^{-16} to 10^{-18} seconds [20].

For protons, consider the following compound reaction example, diagrammed in Figure 2.1. An accelerated proton bombards a ^{7}Li target. The proton is absorbed by a nucleus, distributing all its energy to create the excited ^{8}Be compound nucleus [32]. This intermediate state does not "have memory" of how it was formed, thus several methods of decay are possible. It could emit a neutron and become ^{7}Be or split into two alpha particles.

Direct reactions only involve one or a few target nucleons, and the incident particle is localized in its interaction with the target nucleus. Also called a peripheral process, this reaction involves the projectile interacting mostly with nucleons on the

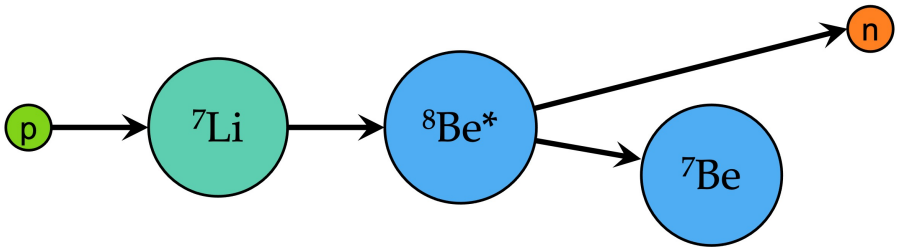

Figure 2.1. An example of a compound nuclear reaction with ^{7}Li(p,n).

surface of the target nucleus. This type of reaction favors higher energies, greater than 20 MeV, as the smaller de Broglie wavelength is better able to interact with nucleon-sized particles [20]. These interactions on the nucleons scale can be modeled a variety of ways, one being the distorted wave Born approximation (DWBA) [33]. One type of direct reaction is proton-neutron charge exchange, where an incoming proton exchanges its charge with a neutron in the target nucleus [34] (see Figure 2.2). At low energies, however, this is relatively unlikely compared to compound reactions.

2.1.2 Deuteron Reactions

The compound nucleus reaction for deuterons occurs the same way as discussed in the proton section. The deuteron directly interacts with the target nucleus and is absorbed, creating a new nucleus of Z+1 and A+2. This is an excited state, which does not "remember" how it was formed, and it rapidly de-excites to a more stable state by decaying. The type of decay depends on the isotope formed and excitation level. Consider a deuteron bombarding a ^{9}Be target, as in Figure 2.3. The resulting

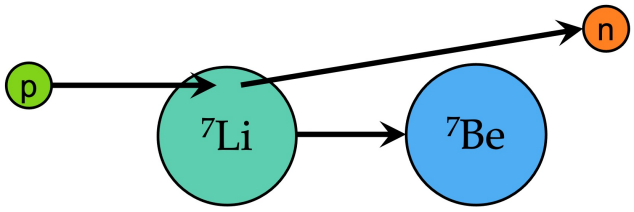

Figure 2.2. An example of charge exchange. A proton impinges on the surface of a ^{7}Li nucleus. After charge is exchanged, the new neutron continues onward, and a ^{7}Be atom results.

compound nucleus is excited ^{11}B, which can emit a neutron, decaying to ^{10}B.

Like protons, deuterons can also interact by way of direct reaction. Deuterons are a loosely bound proton-neutron pair, with a binding energy of about 2.2 MeV. This low energy enables the bond to be broken with relative ease. One such method is stripping [35]: when a deuteron passes very close to a nucleus, one of the two deuteron nucleons can interact with the nucleus and is "stripped" from the other by the nuclear force, as shown in Figure 2.4. It is assumed the proton and neutron have equal chances of interacting. The stripped particle can be absorbed and create a compound nucleus, or else scatter. The other particle can continue either on its path or also at an angle, although the distribution is highly forward focused.

Deuteron breakup can also occur due to the target nucleus' Coulomb field [36–38]. This can occur as the deuteron passes by the target nucleus outside the range of the nuclear strong force but at a distance where it is still affected by the electromagnetic

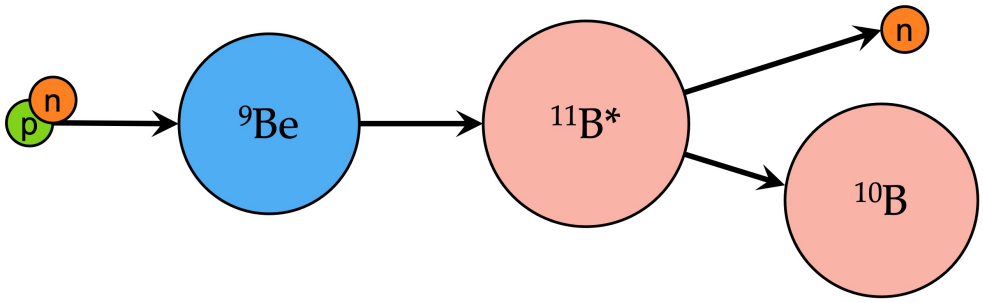

Figure 2.3. A deuteron bombarding ^{9}Be, producing an excited ^{11}B nucleus which emits a neutron in its decay to ^{10}B.

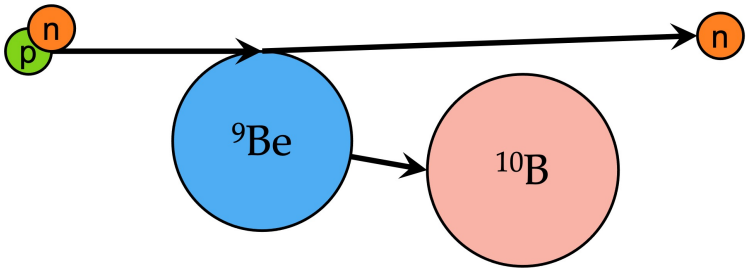

Figure 2.4. In this example of "stripping", the proton of a deuteron bombarding ^{9}Be interacts with the atom and is stripped, forming a neutron and ^{10}B in the process.

force [39] (see Figure 2.5). The loosely bound deuteron is disintegrated as force is exerted on the proton charge, while the neutron continues forward. This reaction has only an estimated quarter of the probability of occurring that stripping has [35].

2.2 The Monte Carlo Method and MCNP

This section discusses the theory of the Monte Carlo (MC) method, cross section libraries, and how both are used in Los Alamos National Laboratory's Monte Carlo N-Particle (MCNP®) code [28].

2.2.1 MC Background

Developed by Enrico Fermi, Nicholas Metropolis, Stanislaw Ulam, and others at Los Alamos Laboratory in the late 1940s, the Monte Carlo method is a statistical approach to simulating reality by sampling distributions that govern what happens in reality, based on probability and random sampling [40, 41]. It is able to provide an answer to a problem in multiple dimensions by describing the phenomenon according to a random number selection. The total solution or picture of the phenomenon emerges from the overall behavior of many individual samples. The more samples,

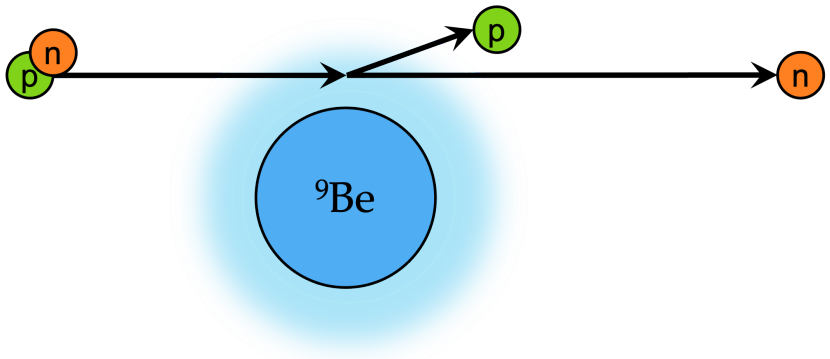

Figure 2.5. Neutron production by Coulombic breakup happens when a deuteron is affected by the Coulomb field (represented by the light blue cloud) of a ^{9}Be atom. The neutron and proton separate and continue on.

the better the statistical confidence of a model. Examples are discussed in the context of MCNP in Section 2.2.3.

2.2.2 Cross Sections

In the most basic sense, a cross section is a quantification of the probability of a certain nuclear reaction event. Suppose the rate of incoming particles a is given as I_a particles per unit time [20]. A target made up of material X is presented with a density of N particles per unit area. The outgoing particles b (usually the particles measured) appear at a rate of R_b. Thus, the cross section σ is quantified as

$$\sigma = \frac{R_b}{I_a N}, \tag{2.3}$$

measured in units of area. The common unit is barns, where 1 barn = 1x10^{-24} cm^2. This is a statistical phenomenon which relates to the quantum mechanical nature of these reactions.

For the purpose of broadly enabling consistent and high-fidelity modeling, cross sections for different reactions can be categorized into data sets according to the target, incident particle, and reaction products. There are many libraries that catalog evaluated cross sections that are based on experimental data, simulations, and model calculations. The cross section libraries investigated in this research are ENDF/B-VIII.0 [42], CP2020 [43], TENDL-2019 [44], and JENDL/DEU-2020 [45]. For simplicity, these libraries are hereafter referred in shortened form as ENDF, CP2020, TENDL, and JENDL (or JENDL/DEU), respectively. A deuteron breakup calculation code by Morrell was also considered [9]. The ubiquitous ENDF library was amalgamated by many institutions from experimental data and calculations. Though it focuses on neutron-induced reactions, it also contains proton tables. CP2020 focuses on charged particles (proton, deuteron, triton, ^{3}He, and α particles) incident

on targets of those same particles, ^{6}Li, and ^{7}Li, with varying maximum energies. TENDL uses the TALYS simulation code to calculate cross sections for nearly every known isotope up to Z=115, for neutron, proton, deuteron, triton, ^{3}He, α, and γ energies up to 200 MeV. The JENDL/DEU library focuses on deuteron cross sections on lithium, beryllium, and carbon targets, calibrating calculations from a custom deuteron reaction code system with a multitude of available experimental data. Based on deuteron breakup theory, Morrell developed a Python program to calculate the expected yield of deuterons on a target from an inputted deuteron energy and target material, benchmarked against experimental data from higher energy above 10 MeV deuteron breakup on a variety of targets.

2.2.3 MCNP

Originally developed for neutron and gamma-ray transport, LANL's Monte Carlo Neutral Particle (MCNP®) transport code has expanded to include electrons and other charged particles, with the "NP" being changed to "N-Particle" [46]. The most recent version, MCNP6, can simulate a host of particle types through a variety of complex geometries [47]. Cross section libraries are an integral part of MCNP simulations as they provide the probabilities used by the MC method. These provide the probabilities used by the MC method. According to the source particle definition, MCNP will track a particle's path and interactions until it stops (e.g., is absorbed) or leaves the system. At each step, the path or interaction is determined using random numbers to chose an interaction based on the chance of that interaction.

Consider a simulation of a proton bombarding a ^{9}Be target, surrounded by a vacuum. The proton is created and sent toward the target. Traveling in a vacuum, there are no interactions until the proton reaches the target. At this point the proton can do one of several things: scatter, get absorbed into a beryllium nucleus, or

otherwise interact with a nucleus. MCNP "rolls a die," picking a random number and the interaction associated with it. The first particle tracked may scatter multiple times, changing direction and depositing energy until it gets absorbed and creates an excited compound ^{10}B nucleus. What happens as a result of that absorption is also determined by probability as well. The nucleus could emit a neutron which is then tracked until it leaves the system or initiates a new reaction. The next particle may get absorbed as well, but this time the ^{10}B nucleus simply de-excites by emitting a gamma ray. Meanwhile the third particle sent never gets absorbed and exits the system after a few scatters. Combining and averaging these interactions provides a solution to the problem of protons bombarding a ^{9}Be target.

MCNP can keep track of specific actions in a so-called "tally". One such tally is when a certain particle, say a neutron, crosses a specific surface. This tally is weighted according to the number of source particles and the number of neutrons which cross the surface. MCNP has a large variety of different tallies [28].

2.3 Optimization Methods

Optimization is the process of searching for the best solution to an objective function. Methods are numerous. One way to differentiate among these methods is to sort them into three groups: deterministic, stochastic, and enumerative [48]. Deterministic methods follow mathematical definitions to reach a solutions, like taking the derivative to determine the slope at a point, and searching in the direction toward a minimum. These are limited to problems with mathematically defined phenomena. Enumerative methods involve stepping through every possibility within a parameter space to land on a global extreme. These methods, while thorough, can be incredibly time-consuming with many parameters. Stochastic methods use random sampling to test many different points in a parameter space to pinpoint the best solutions, and

can be used in conjunction with the other two. This family of stochastic methods is potentially useful for nuclear reaction processes and MCNP as different combinations of model parameters can produce a wide range of results that are too numerous to explicitly list.The approach chosen for optimization is a genetic algorithm, and will be discussed in more detail in Section 3.3.2.

III. Methodology

The goal of this research is to conduct a preliminary investigation into optimizing a target configuration (as defined by a set of materials and corresponding thicknesses) to maximize neutron production from a charged particle beam. To accomplish this, optimization studies were conducted by stochastically designing MCNP [28] simulations with parameters from Dakota [29] and evaluating the results. To build confidence in the MCNP simulations, the models of the various reactions involved – which depend on the cross section libraries – must be validated against literature. This chapter will discuss the steps and reasoning taken to get the final optimization code, including the potential sources of error and uncertainty. The validation will be discussed first, followed by the implementation of the Dakota optimization.

3.1 MCNP Validation

This section will describe the process for validating MCNP models of the various reactions. Specifically, the cross section libraries driving the model results will be investigated. The need for validation is obvious: the simulations of basic reactions must be evaluated before relying on the outputs of the optimization code.

The first step in validation was choosing the reactions and gathering literature on those reactions for comparison. Then, an MCNP model was developed to perform the simulations in a manner reflecting the experiments in the literature. The simulation results were then be compared to the literature for validation. The output neutron energy spectrum was plotted in comparison with the literature to allow shape and magnitude comparison. Where applicable, the total neutron production was also considered, particularly if the spectrum shape was in disagreement. Some literature used only arbitrary units when reporting the neutron spectrum; in these cases the

shape and, if applicable, total neutron flux were compared.

A quantitative statistical comparison was not performed. However, the goal was to identify the cross-section library that most closely represented reality for this study, not suggest detailed improvements for any given library.

3.1.1 Choosing the Reactions

After (and during) an extensive literature review of various materials and previous neutron production capabilities, a list of suitable materials was compiled based upon availability and commonality. In each of these datasets, a stationary target made of a given material was irradiated with either protons or deuterons and the resulting neutrons were measured. The reactions, energies, and corresponding literature is summarized in Table 3.1. Materials were considered suitable if they had high neutron production rates for incident particle energies below 8 MeV, but the energies of particular note were 2 and 5 MeV, as these are what Gamble II and Mercury can produce, respectively. In one case, a beam energy outside the 8 MeV limit was considered (16 MeV deuterons on beryllium) due to the availability of multiple high-quality datasets. [49, 50]. Many experiments used energies much larger than the present range [51] as higher energies increase neutron production.

Proton Reactions

The materials considered for the proton reactions are lithium and beryllium. Lithium is a common material used for neutron production [25]. The threshold for the ^{7}Li(p,n) reaction is 1.881 MeV [52]. This reaction is somewhat unique in that at low energies near the threshold, the neutron angular distribution peaks around 25-30° off the incident beam axis [52]. Beryllium is also a common material for neutron production in various applications, such as boron neutron-capture ther-

Table 3.1. Reactions Explored for MCNP Validation

Reaction	Energy (MeV)	Corresponding Paper
Li(p,n)	1.912	Lederer (2012) [52]
	2.52	Lefevre (1969) [53]
Be(p,n)	3.7	Howard (2001) [11]
	5.0	Ibid.
D(d,n)	0.2	Gillich (2010) [54]*
	2.0	N/A
Li(d,n)	2.0	Jones (1974) [55]
Be(d,n)	2.6	Meadows (1993) [56]
	7.0	Ibid.
	8.8	Weaver (1973) [30]
	16	Harrig (2018) [24]
		Meulders (1975) [50]
C(d,n)	5.0	Tajiri (2014) [31]

apy [13, 14]. The threshold is 1.749 MeV for the ^{9}Be(p,pnα)α reaction and 2.06 MeV for ^{9}Be(p,n)^{9}B [11]. However, it can have detrimental health effects [57], which must be considered for future development. Another material identified, but not considered for this optimization, was vanadium. The ^{51}V(p,n)^{51}Cr reaction has a threshold of 1.565 MeV [58–60], but its production below E_p=5 MeV was negligible compared to lithium and beryllium. At higher energies this reaction may have use.

Deuteron Reactions

The materials considered for the deuteron reactions include deuterium (in the form of deuterated polyethylene), lithium, beryllium, and carbon. Also identified but not used in the optimization were oxygen, aluminum [61], tantalum [39, 50], and titanium [39]. Tritium was considered, but due to cost and safety issues it was not investigated further. As in the proton reactions, the light materials lithium and beryllium are common materials for neutron production with deuterons [50, 62]. Deuterium is useful because the D(d,n) reaction produces an energy peak from the Q value of 3.3 MeV. Also, it has a good cross section even in the keV energy range [54]

and could be used on the back of a target to react with low energy deuterons emerging from earlier layers. Carbon does not have the toxicity of beryllium or the cost of deuterium [31], making it a useful, cheap target.

3.1.2 MCNP Validation Models

The MCNP 6.2 [63] code was used for all simulations (for both the validation and optimization), which were run on high-performance computing (HPC) clusters. The code was established on both Bridgman and Mustang systems enabling their use throughout this research. Bridgman, AFIT's system, consisted of 10 nodes with 16 processors per node. Mustang, one of the Air Force Research Lab's HPC systems, consisted of 1176 computing nodes, each with two 24-processor cores operating at 2.7 GHz [64].

The MCNP model is a simplified version of the experimental setup commonly used in the literature. It consists of a source, a target cell, and a "detector" surface (for the surface tally), as shown in Figure 3.1. The source is a mono-directional, mono-energetic disk source with a radius of 1 cm, intended to model a "pencil beam" [43]. The source was defined using either protons or deuterons depending on the reaction being modeled and had a uniform geometric distribution within the disk. The beam was co-axial with the x-axis (as indicated by the centerline in Figure 3.1).

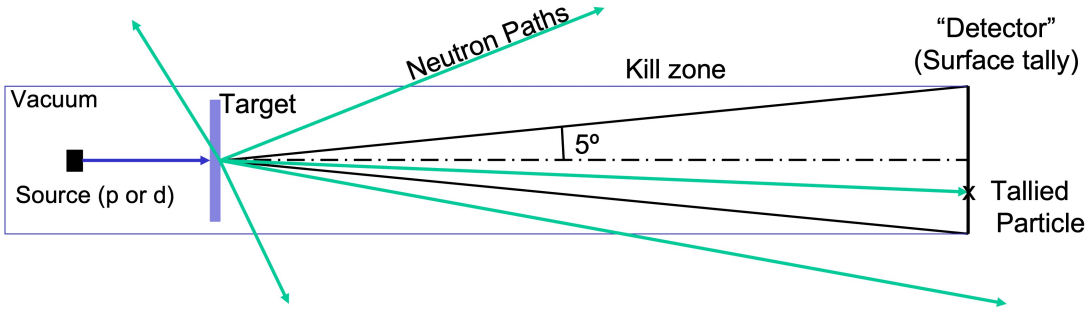

Figure 3.1. The MCNP validation model covered a solid angle corresponding to 5°, a common setup in literature.

The target was a cylinder with a 5-cm radius located 5 cm away from the source, coaxial with the x-axis. This positioning ensured all the source particles would hit the target while providing material for internal scattering if applicable. The target thickness (the height of the cylinder) was determined by the particular reaction and literature, although it was always much less than 1 cm. The stopping distance was calculated for each material at a range of energies using SRIM [65], discussed in Section 3.3.2. These distances were used as minimum thicknesses for the MCNP simulations, as well as for confirming the target thicknesses from the literature measurements. Often, the thickness used in a validation run was twice to ten times greater than the stopping range, common for thick targets designed to maximize neutron yield.

Each target consisted of purely the most common isotope of a given material. For example, the carbon targets were entirely made of ^{12}C. Lithium had the most abundant natural second isotope, ^{6}Li, at 6%, but the cross sections for the proton and deuterons at the energies considered was significantly lower than for ^{7}Li. ^{9}Be is the only naturally occurring isotope fo beryllium, and ^{13}C only comprises of 1% of natural carbon. Impurities in targets of these elements would depend on budget in practice, but for this exercise they are neglected. The one or so percent difference between pure and lab materials is much less than the statistical uncertainties of the MCNP models, and the differences between the MCNP results and experimental values. Similarly, the CD_2 is assumed to be 100% deuterated.

The detector surface was the far circular face of the boundary cylinder (the right side of the surface in Figure 3.1). For the validation simulations, the detector surface covered a $\pm 5^\circ$ solid angle from the origin. This configuration was chosen to best match with the measurements in the literature that mostly used small detectors, which covered approximately 5°. Many papers also had measurements at different

angles from the x-axis, in 5-10° increments, and the neutron flux did not appreciably change between those increments, so this 5° was a logical detector surface extent.

One downside to this small solid angle is the low statistics. The solid angle, calculated according to the simplification $\Omega = \frac{1}{2}(1 - \cos\theta) \cdot 4\pi$, is 0.024 sr, just 0.2% of the sphere. Many particles are needed to produce reasonable statistics, and some reactions are better than others. This means the simulations may take up to several hours. The "*nps*" (number of particle histories to be run before terminating) values ranged from 5e7 to 5e9 to ensure each reaction achieved reasonable statistical uncertainties ($< 10\%$). If fewer neutrons are produced by the target per source particle, then more particles are needed to achieve comparable uncertainty. This result indicates that a reaction that requires a higher *nps* value is generally less desirable.

Finally, the model used the surface current tally type (F1:n) [28], which counts the number of particles crossing a surface (in this case the detector surface) and weights them according to the total number of source particles. These were also binned into discrete energy groups and scaled with a multiplier card (FMn) to normalize the units to those used in the literature. The F1 tally card has default units of *crossing particle/source particle*. For example, the F1 output units for modeling a (p,n) reaction would be neutrons per source proton. The most common unit reported in literature is 10^9 n/μC/sr/MeV. Since the F1:n tally defaults to units of neutrons per source particle, the MCNP tally must be scaled with the FM card. The charge of a proton or deuteron is $1.6022{\cdot}10^{-13}$ μC, so if the bin size is 1 MeV then the unit conversion using a 0.024-sr solid angle is as follows:

$$\frac{n}{p} \cdot \frac{p}{1.6022 \cdot 10^{-13}\ \mu C} \cdot \frac{1}{0.024\ sr} \cdot \frac{1}{1\ MeV} \cdot \frac{10^9}{10^9} \;=\; 260059 \cdot \frac{10^9\ n}{\mu C \cdot sr \cdot MeV},^{1} \quad (3.1)$$

[1] A calculation early in the research used a solid angle of 0.0241 sr, which yields a multiplier of 258980, just a 0.4% difference from 260059 and well within significant digits. The 258980 multiplier

where n refers to the number of neutrons produced per proton p. This number can be scaled to bin sizes other than 1 MeV by dividing by the bin size. For example, if a reaction used 0.25 MeV bins, the multiplier would be 1,040,236. The specific bin size (all equal widths) and range for each reaction was estimated from the literature spectrum and adjusted as needed.

3.2 The Comparison Process

When each run was complete, it could then be compared to the corresponding literature. The number of particle histories run could be tweaked if needed to produce a statistical uncertainty of less than 10% for each energy bin. (Since the total tally is a summation of each bin, the uncertainty on the total neutron flux is much smaller.) A 5% uncertainty was initially the target, but this was not attained for all energy bins for some cases. Results were plotted alongside the experimental data. However, since the goal of this research is to find the highest neutron flux with a multi-layered target and not create a specific spectrum, the total neutron production was also considered for some reactions. The total neutron production from MCNP was reported as the sum of the bins. If the bin width was not 1 MeV in a run, the total was multiplied by the bin width to normalize. If the literature did not have a specific total neutron production number, the literature spectrum was integrated. Spectrum results are also plotted with the statistical error bars for each energy bin. Numbers are compared both quantitatively and qualitatively.

was used for the majority of the validation runs.

3.3 Optimization

3.3.1 Optimization MCNP Models

The MCNP model for the optimization portion includes two main alterations from the validation model. First, the detector angle was changed from ±5° to ±30° (Figure 3.2) to boost statistics. Each MCNP validation run at 5° took on the orders of minutes to hours to get acceptable statistics. Multiplying that by the few hundred runs the optimization software will need to find the solution results in a prohibitive runtime. The change to 30° reduces the number of particles needed to get within 5-10% total neutron production uncertainty by about 1000. This reduces the runtime of the whole process, while retaining the uncertainty targets for the results. This may actually be more representative of the NRL experimental setup as an NRL test object size may be much larger than a small detector and be located at a shorter distance than was done in the validation literature experiments where additional distance was used to improve neutron spectroscopy and refine angular distributions. However, this introduces an issue in that there will be a non-uniform fluence across this angular distribution, a factor that was not explored in this work.

The second change was the addition of two target layers, for a total of three. The thicknesses and material composition of these three layers were chosen by the optimization software, as described in Section 3.3.2. Otherwise, the model is the same, consisting of a 1-cm radius disc source, cylindrical targets, surface tally, and kill zone.

3.3.2 Dakota Optimization

Overview of Dakota

Dakota is a software suite developed by Sandia National Laboratory (SNL) that serves as an interface for simulation codes and iteration methods [66]. The software

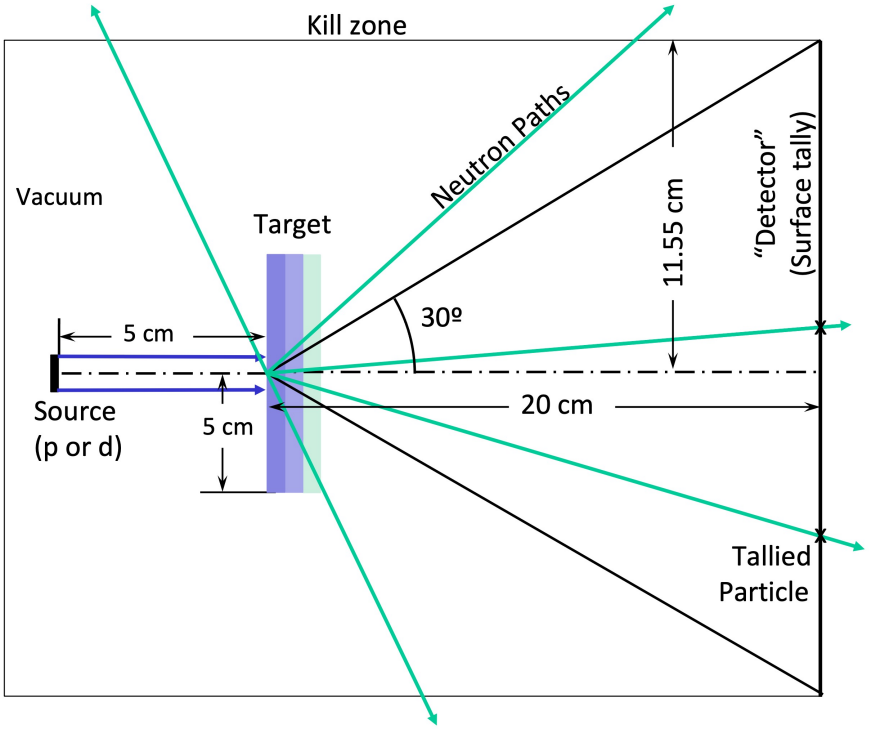

Figure 3.2. The MCNP validation model covered a solid angle corresponding to 30°, with a three-layer target.

allows for a wide range of customization, from uncertainty analysis to design optimization, as used in this research. It runs simulations based on a discrete or continuous user-defined range of parameters, keeping track of each simulation and changing variables accordingly. Depending on where the optimization was run, different versions were used: version 6.8 on Bridgman, 6.11 on Mustang, and 6.14 on the author's personal computer. The differences between them were minimal, and did not noticeably affect the running nor results.

Optimization Method: SOGA

The single objective genetic algorithm (SOGA) optimization method was chosen because it is good for multiple discrete variables (such as the specific materials considered for the target), derivative-free (a MC method was used to model the reactions,

not equations), and bound constraints (minimum and maximum thicknesses) [66]. A genetic algorithm (GA) (an evolution-based algorithm) samples a parameter space first with a set of parent characteristics, or genes. Crossovers (combining genes) and mutations (altering genes slightly) are performed, and the new population is evaluated. The fitness of each member of the new population is assessed and the best are chosen to be parents of the next population. The program loops until a user-defined convergence criteria is reached [67]. SOGA is also a conceptually straightforward implementation of a GA that is particularly strong in global optimization.

Settings and Parameters

The two parameters that were changed throughout the optimizations were the target layer material composition and the thickness of each layer. The materials are chosen from a set list, as outlined in Section 3.1.1. Dakota chooses the thickness by assigning an integer from 1-100, which represents the percentage of the maximum thickness of a layer. This was done to simplify the optimization for use with Dakota. If a continuous range of thicknesses was used, the number of possible values would depend on the magnitude of the maximum thickness and the significant figures specified for the range. Since this varies between target materials, and the thicknesses and materials were were varied independently, the percentage of the maximum thickness (in steps of 1%) was chosen to represent the range of thicknesses. A script converts the percentage to centimeters according to the maximum thickness for the particular layer's material and fills in the template MCNP model. This maximum thickness is the maximum distance a particle of a particular energy is expected to travel into a certain material. If a particle is not expected to travel beyond a certain distance, then it is unnecessary to have the optimization explore thicknesses beyond this. Additional thickness or layers would reduce the number of neutrons that pass through and in-

crease material cost. Justification for this is discussed in the next paragraph. These maximum thicknesses were found using SRIM [65] calculations for each reaction in Table 3.1. Approximately five percent was added to each SRIM result to provide a buffer. The values from SRIM and the actual maximum thickness are summarized in Table 3.2.

A study was conducted for a single-layer target to compare the thickness of the MCNP model that produces the most neutrons (as determined via Dakota) to the SRIM thickness. Dakota was used to step through a range of thicknesses, outputting the forward neutron production for each run. Somewhat arbitrarily, 8 MeV deuterons on ^{9}Be and 2.75 MeV protons on ^{7}Li were chosen for this, with the results of the Be(d,n) reaction displayed in Figure 3.3. As the thickness increased, the neutron production increased until it reached a maximum value at SRIM's projected range. The neutron production stayed relatively constant beyond that point, decreasing slightly as the thickness increased. It is assumed that this is due to the increased neutron scatters that could occur within the material, increasing the chances of a neutron

Table 3.2. Materials and Maximum Thicknesses Used in Optimization

Incident Particle	**Energy**	**Material**	**SRIM Range (μm)**	**Maximum Thickness Used (cm)**
Protons	2 MeV	Li	159.08	0.017
		Be	48.52	0.005
	5 MeV	Li	785.20	0.083
		Be	233.61	0.025
Deuterons	2 MeV	Li	102.54	0.011
		Be	32.07	0.004
		CD_2	47.08	0.005
		C	24.78	0.003
	5 MeV	Li	466.82	0.050
		Be	141.37	0.015
		CD_2	210.01	0.022
		C	109.41	0.012

changing direction or becoming embedded in the material. The Li(p,n) reaction showed similar trends. This demonstrates confidence in the SRIM calculations for the material thickness range used in the optimization.

3.3.3 Code Suite: Putting It All Together

The code suite is outlined in Figure 3.4. First, a run-specific shell script initializes the options unique to each run — creating a new work directory, and defining the particle, energy, and number of particles (nps) for MCNP to use, as well as the run IDs — and writes these to the parameters file and other input files. Next it submits the job to the PBS system, which runs Dakota with the Dakota input file.

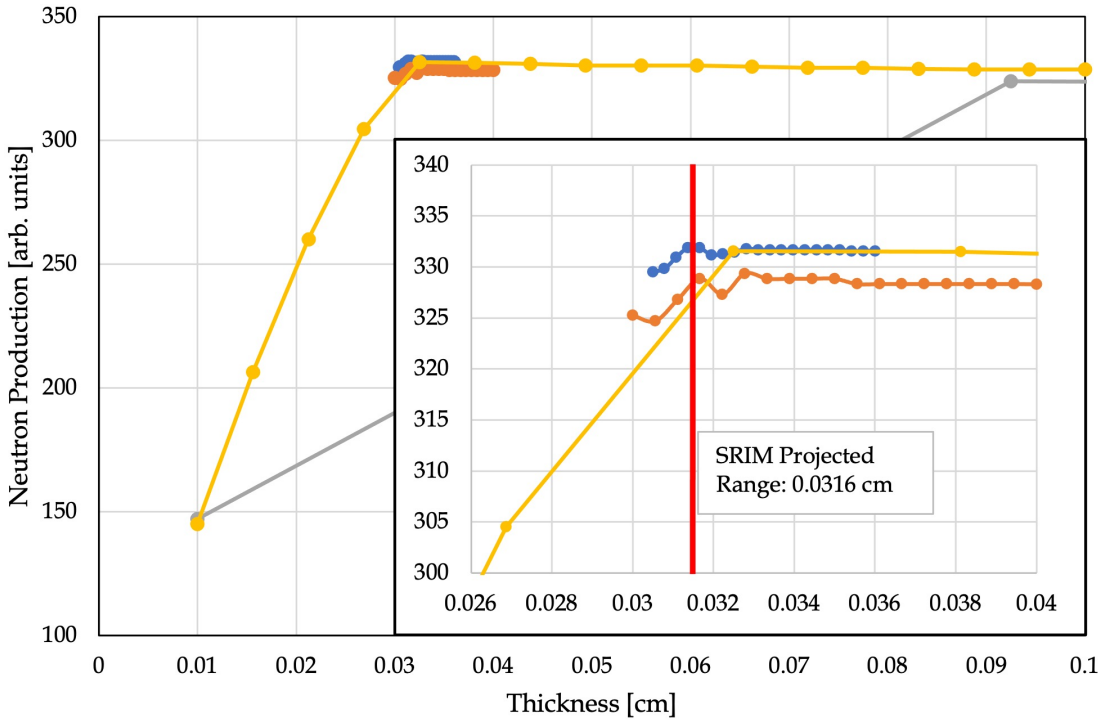

Figure 3.3. The Dakota thickness scan shows the maximum neutron production does occur at the SRIM projected range. Four runs were completed, each in finer steps. The first, shown as the gray points, went to 1 cm, and showed the slight decrease in forward neutron production as thickness increased. The yellow also shows this trend on the short range of 0.1 cm. The orange and blue, as shown in the zoomed inset image, are the finest scope, and the difference between the two is due to different seeds, but they are within the statistical uncertainty of about 5%.

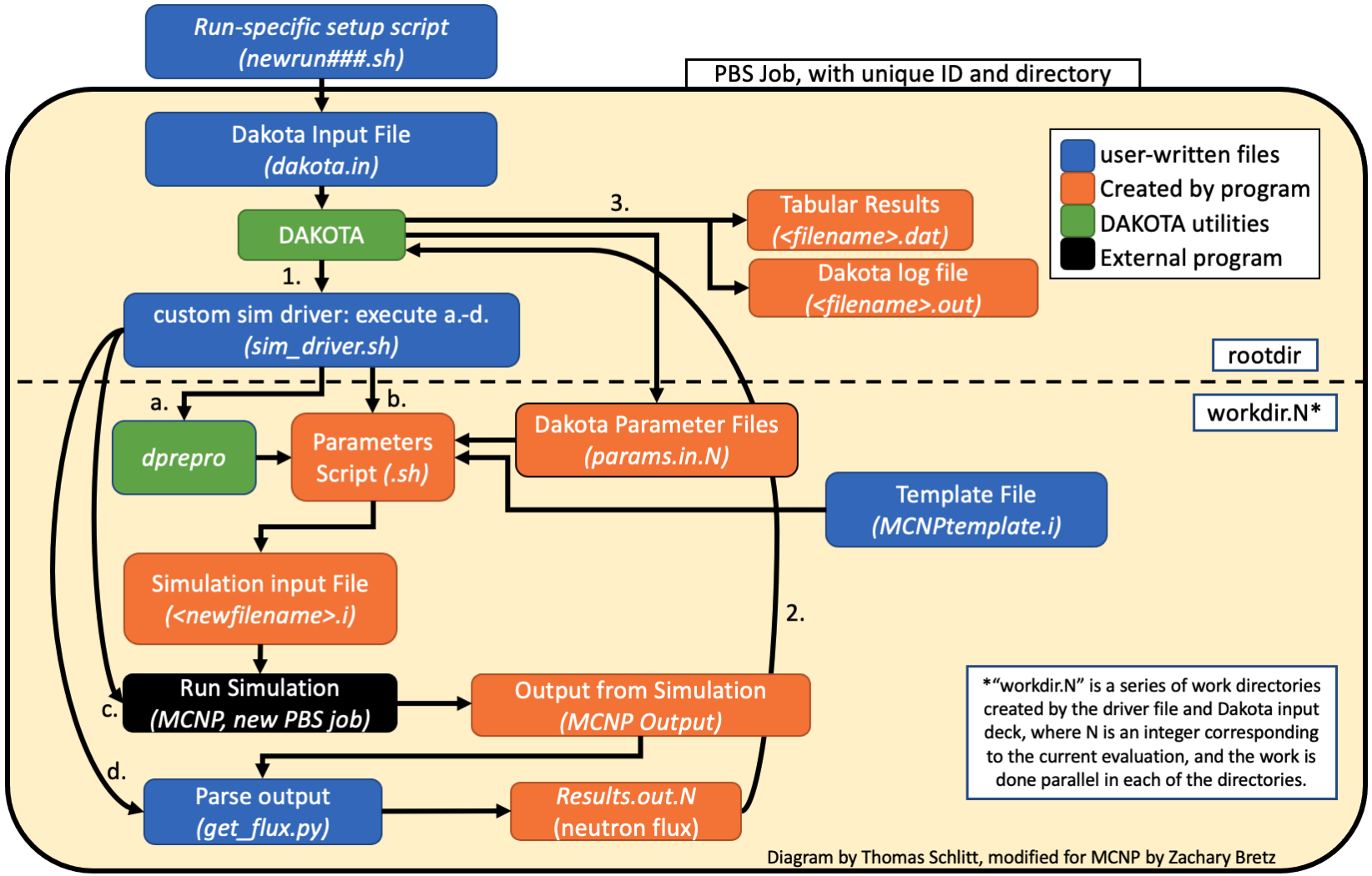

Figure 3.4. This figure lays out the process of beginning a new run with various settings in the *newrun###.sh* file and running a new Dakota input file, which loops through MCNP runs with different parameters until convergence is reached.

Dakota loops through three steps for each evaluation, indicated by the numbers in Figure 3.4. These evaluations can be done in parallel, as defined by the Dakota input file. The first step (1.) is running the custom simulation driver, which has three main sections: pre-processing (a. and b.), execution (c.), and post-processing (d.). The driver is run in a work directory unique to each evaluation N (named *workdir.N*, explained in Figure 3.4). In pre-processing, the driver runs the Dakota utility *dprepro* (a.) to replace the evaluation's parameters — layer material and thicknesses — in a certain file. In this case, *dprepro* edits the intermediate "Parameters Script," which is not to be confused with the Dakota parameter files used by *dprepro*. The driver runs this Parameters Script (b.), which calculates the actual layer thickness from the percentages given by Dakota and correctly formats the MCNP input file. The execution stage of the driver submits the MCNP job, which runs MCNP and saves the output (c.). When the driver sees that the output is finished, it runs a Python script to parse the output (d.) and saves it to a file Dakota can read (2.). The output is the objective function result and part of the population described in section 3.3.2. Dakota aggregates these results from each evaluation, chooses new parameters (3.), and the process loops until convergence. The results are saved in several output files. Example files for the whole process are included in Appendix A.

IV. Results

4.1 MCNP Model Validation

This section summarizes the results of the MCNP model validation of the proton- and deuteron-induced neutron production reactions models, which will be used for the target optimization. Neutron energy spectra from the MCNP binned output tallies are plotted in comparison with the corresponding literature (where applicable). In some cases, the literature has arbitrary or relative neutron production units: these are provided on a secondary axis and scaled to similar magnitudes as the MCNP outputs for comparison of the spectrum shape. Since MCNP reports tallies according to energy bin, the following plots consist of points at the center of the bin. The bins, except where specified, are all the same width within each plot. Statistical uncertainty is represented by error bars.

4.1.1 Proton Reactions

4.1.1.1 Protons on Lithium-7

The ^{7}Li(p,n)^{7}Be reaction was evaluated at incident proton energies of 1.912 and 2.52 MeV and compared to the works by Lederer et al. and Lefevre et al., respectively [52, 53]. At energies just above the threshold of 1.881 MeV, the integrated neutron intensity peaks at an angle about 30° off the centerline [52]. A 5° detector angle yielded almost no neutron tallies for a reasonable runtime of a few hours, which makes sense as the yield at 0° is quite small. Thus, for the 1.912 MeV reaction, a detector angle covering 30° was used. The Lederer 0-30° measurements were summed, plotted on the secondary axis, and scaled to compare to the MCNP results in Figure 4.1. The other literature found in addition to Lederer for this reaction and energy had "arbitrary" or "relative" units for the neutron production [68–70], so only

the shape was compared. The MCNP result is slightly shifted to the right, but the general shape is similar.

The detector surface is a key difference between how the MCNP model and the Lederer experiment were set up. As described earlier, the MCNP model "detector" – the surface which tallied neutron crossings – was a large circle covering 0-30° 3.2. Lederer et al. used a 3.89-cm-diameter detector 71.9 cm away from the lithium target, for a small angle spread of about ±1.5°. This was moved in an arc about the target for each angle, with the change in solid angle at each measuring point accounted for with a correction factor. The Lederer neutron spectrum data includes ±2.5° of the angle listed; thus, the 30° bin includes 27.5° to 32.5°, whereas the MCNP model had a hard cutoff at 30°. Lederer used the single detector, with an angle coverage of ±1.5°, but this small angle difference – 30° versus 31.5° – was assumed to have only a small effect. Alternatively, the results could be compared according to the slope from the 0.07 to 0.10 MeV part of the spectrum by raising the magnitude of the Lederer

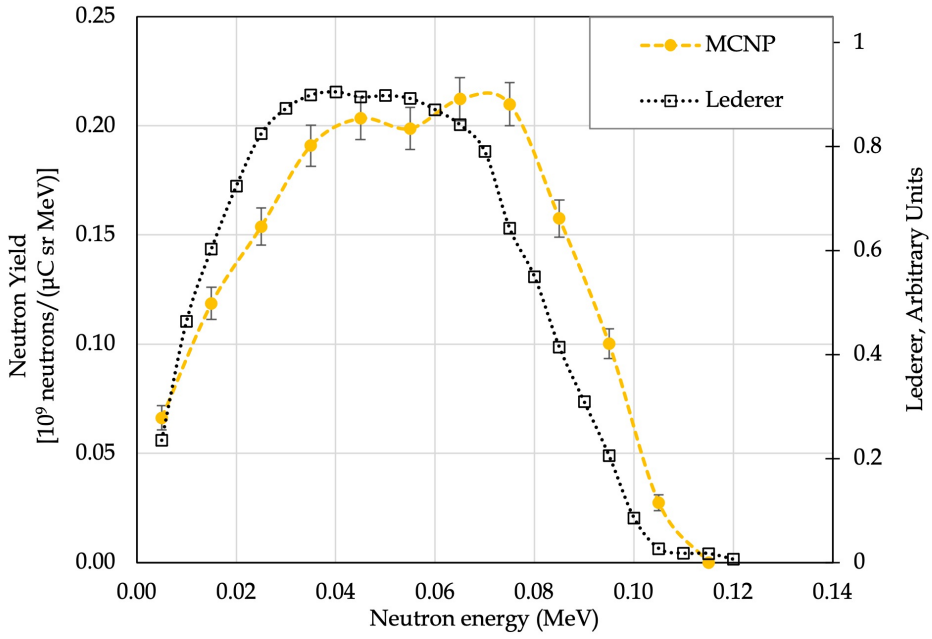

Figure 4.1. The MCNP results for the 1.912 MeV protons on lithium are shifted to the right of the Lederer data but show a similar shape.

data, as in Figure 4.2. In this case, the MCNP simulation appears to underpredicts the data below 0.06 MeV, which is similar to what happens with two of the Be(d,n) reactions in Section 4.1.2.2. Based on the shape similarity, however, this is likely not the correct interpretation.

The 2.52 MeV simulated spectrum matched closely to the Lefevre data [53], but it had an additional slight peak around 0.7 MeV and was shifted slightly to lower energy. This is plotted with the 1.912 MeV data in Figure 4.3. Lefevre did not report experimental data below 0.3 MeV, so it will not be considered in the comparison. Like the 1.912 MeV run, this MCNP model was done with a detector that covered 0-30°. The Lefevre experiment covered approximately +/-6°. The slight variations between the two could be because of this angle discrepancy. Higher energy neutrons are generally forward focused [71], while the production from protons of energies closer to the threshold are not. Thus, the slight bump at 0.7 MeV may not be because of

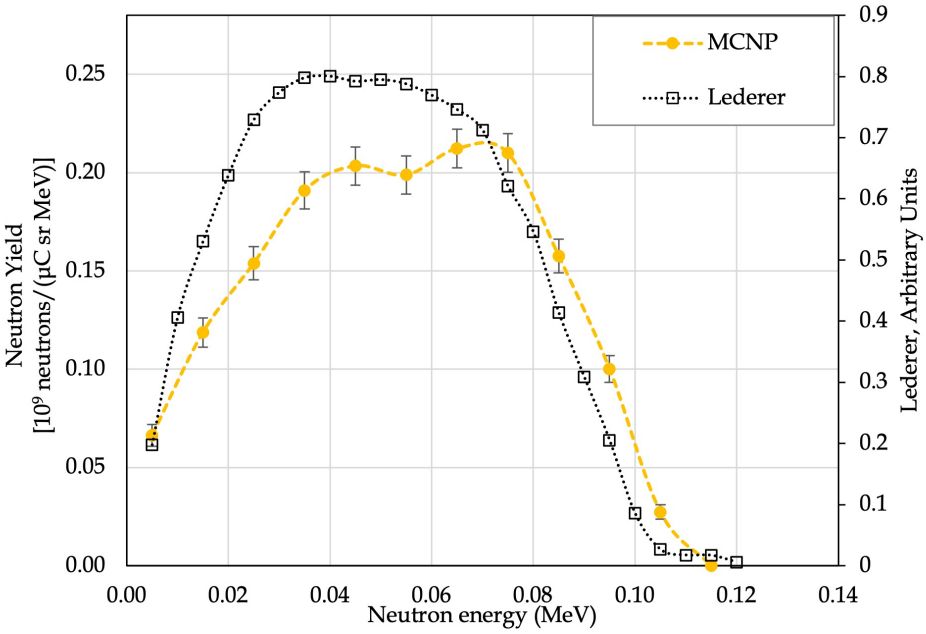

Figure 4.2. If the Lederer data magnitude is increased to align with the edge of the MCNP results for the 1.912 MeV protons on lithium, MCNP underpredicts neutron production below 80 keV, much like the Be(d,n) reactions in Section 4.1.2.2.

the angle discrepancy but more so a difference in the cross section library. The wider angle could capture more lower-energy neutrons, which could contribute to the shift. The tally cosine card may have been a better way to go about this, as will be discussed in the conclusions of Section 5.1.

There is a large difference between the neutron spectrum from the 1.912 and 2.52 MeV protons. The threshold for the ground state reaction is 1.881 MeV and results in 0° neutrons with energies of 0.03 MeV [72]. The first excited state threshold is 2.372 MeV [72] and results in neutrons of 0.65 MeV. Below 2.5 MeV, fewer than 1% of neutrons are from the excited state reaction [73]. This increase in neutron energy between the two reaction types explains the ∼0.5 MeV shift in main peaks shown in Figure 4.3.

The different cross sections also explain the additional magnitude increase of neutron production between the two energies. At $E_p = 1.912$ and below, the cross section

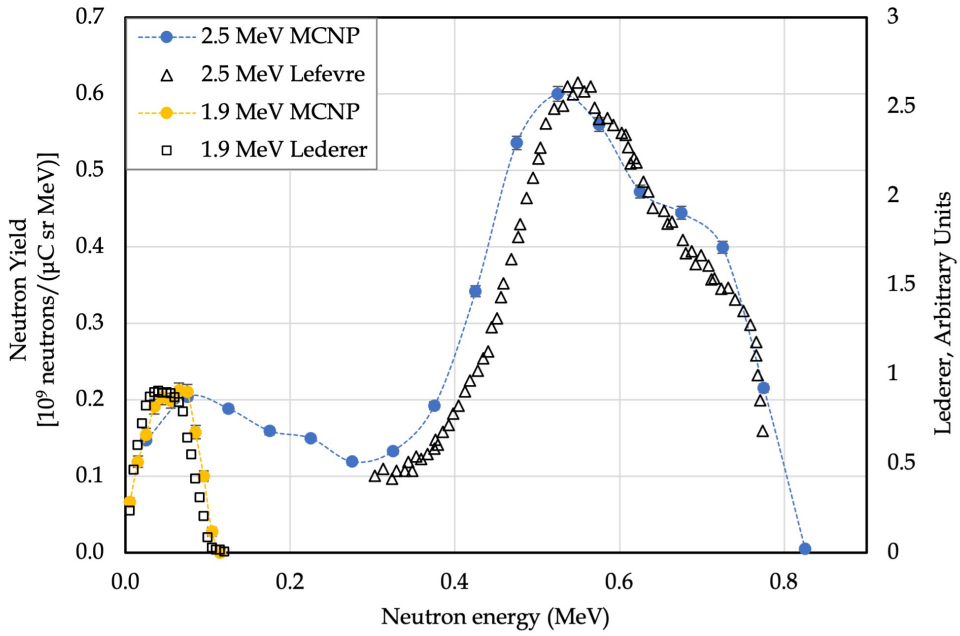

Figure 4.3. The MCNP results for the 2.52 MeV protons on lithium are shifted to the right of the Lederer data, but shows a similar shape. Statistical error is small than the marker size. The 0.6 MeV increase from 1.912 to 2.52 MeV in incident proton energy greatly increases the average neutron energy and total neutron production.

is approximately 250 mb, exponentially decreasing as the threshold is approached, as shown in Figure 4.4 [74]. Below 2.5 MeV, there is a peak of 600 mb at E_p ~=2.25 MeV. The initial 2.52 MeV protons deposit energy within the bulk material and drop closer to the 2.25 MeV peak, increasing their chances of interacting to produce a neutron. The cross section drops off after 6 MeV, near the maximum of Mercury, meaning proton energies up to that value will most efficiently produce neutrons. A study above 2.52 MeV was not conducted in this research and is recommended in future work.

4.1.1.2 Protons on Beryllium-9

The ^{9}Be(p,n) reaction was evaluated at incident energies of 3.7 and 5 MeV, each compared to Howard [11]. This reaction shows significant discrepancy between the simulated spectra and the literature measurements. The MCNP model was set up

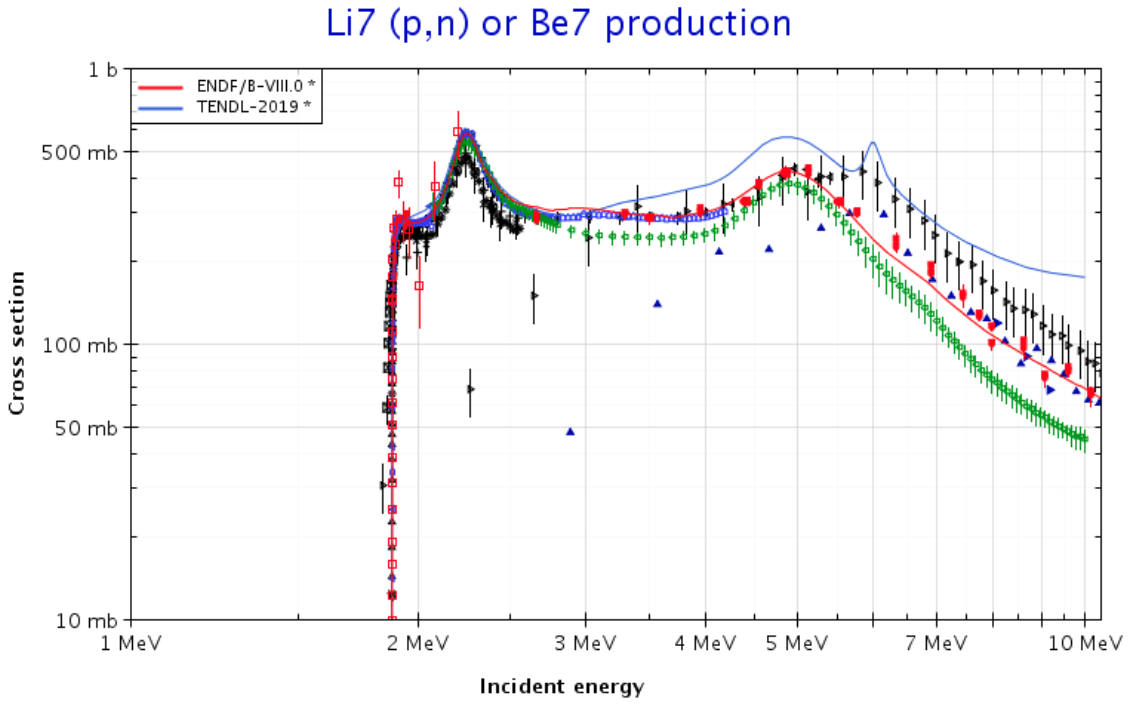

Figure 4.4. The ^{7}Li(p,n) reaction cross section has a peak around 2.25 MeV and hovers around 300 mb elsewhere below 5 MeV to the reaction threshold of 1.881 MeV [74]. Various experimental data points are included but not represented in the legend.

with the 5° detector surface using 10^9 particles for each run. The 3.7 MeV run – spectrum plotted in Figure 4.5 – produced a peak at about 1.1 MeV with the ENDF/VIII library, which does not exist in the Howard data. However, two peaks at about 0.6 and 1.65 MeV from the model using the ENDF library did match within a tenth of an MeV.

The TENDL library did not perform well. The data diverges slightly below 0.25 MeV, Howard trending toward zero and MCNP producing more counts. In calibrating their system, Howard et al. used the Al(d,n) above ∼0.25 MeV. Due to the ∼0.25 MeV, the neutron production drops off significantly, increasing the uncertainty. Thus, below 0.22 MeV they used literature to calibrate, conceding its potential inaccuracy. Their total error above 250 keV was estimated to be less than 10%, and below 250 keV it was 20%. However, even with this error, the MCNP spectrum is far outside this range, often with a 20-30% discrepancy.

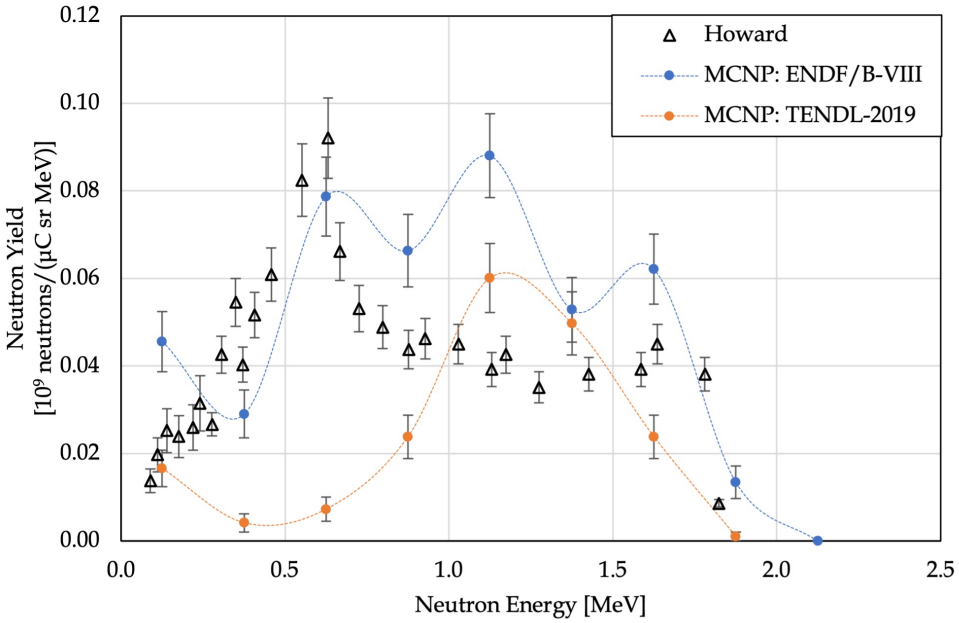

Figure 4.5. The ^{9}Be(p,n) reaction was modeled using both the ENDF/VIII and TENDL-2019 libraries and compared to the results of Howard et al. for 3.7 MeV incident protons [11].

The $E_p = 5\ MeV$ simulation, however, incorrectly predicted the lower energies (see Figure 4.6). The peak at about 2.65 MeV agreed with Howard quite well. MCNP had the other peak shifted to about 1.1 MeV, whereas the Howard data placed it around 0.5 MeV. The TENDL library greatly underperformed.

The total neutron yield for both energies was also compared and summarized in Table 4.1. Howard reported the total yield in Figure 17 of that paper. The data from Figure 12 of the paper was integrated over to compare to the Figure 17 value as confirmation. The total production from the MCNP simulations was also calculated. The value from each bin was summed and multiplied by the bin size. The percent difference was then calculated (according to $\frac{Howard\ -\ MCNP}{Howard}$). The 3.7 MeV run produced over 40% more neutrons per μC per steradian than the Figure 17 Howard data, largely due to the middle peak. This makes sense, as the MCNP data has the extra peak at 1.2 MeV. The 5 MeV total yield, however, was only 0.54% different than the Howard reported yield. The higher proton energy at 5 MeV is

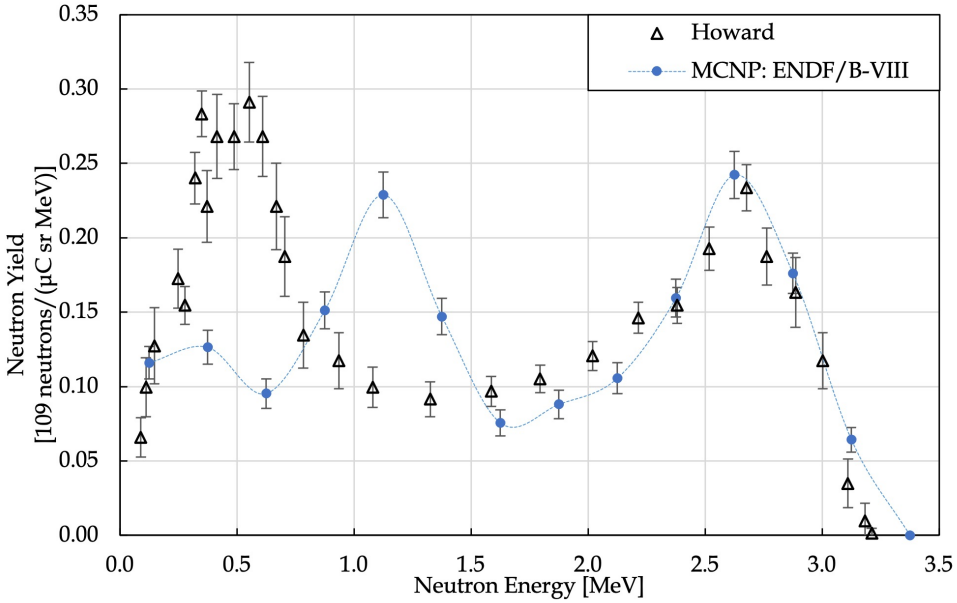

Figure 4.6. The ^{9}Be(p,n) reaction was modeled using both the ENDF/VIII and TENDL-2019 libraries, and compared to the results of Howard et al. for 5 MeV incident protons [11].

modeled adequately by MCNP.

Table 4.1. Total neutron production from the Be(p,n) reaction, in units of 10^9 n/μC/sr

E_p (MeV)	Howard Fig. 17 [11]	Howard Fig. 12 (Integrated) [11]	MCNP Bin Summation	% Difference
3.7	0.076	0.079	0.109 ± 4.9%	42.72%
5.0	0.442	0.461	0.444 ± 2.4%	0.54%

4.1.2 Deuteron Reactions

This section summarizes the results of the simulations of the Li(d,n), Be(d,n), C(d,n) and D(d,n) reactions at various energies. How well each cross section library compares to literature for both the outgoing neutron spectrum and total neutron production in the forward direction is discussed. The ENDF libraries do not have cross section data for deuteron-induced neutron production, in which case MCNP defaults to using physics models if specified. These physics models are aimed at higher energy interactions (>20-50 MeV) and also not accurate. Instead, the JENDL/DEU-2020 and CP2020 libraries were used for these reactions.

4.1.2.1 Deuterons on Lithium

The ^{7}Li(d,n) reaction was evaluated at 2 MeV and compared to Jones [55]. The MCNP simulation used 10^9 particles and the 5° detector range, producing statistical errors ranging from 15 to 40% in individual bins but 5% in the overall yield. Jones measured the neutron production above 2.5 MeV at angles from 0-90°. To integrate for the total flux and to calculate average energies, Jones et al. extrapolated two ways: A) horizontally finishing the spectrum and B) down to the origin (indicated by thick dashed lines in Figure 4.7) [55]. As will be seen later, Weaver [30] also uses these two methods. The MCNP results might suggest a third way: C) carrying the line

upward at an angle. This would need more further investigation to make a definitive conclusion.

The MCNP spectrum using JENDL/DEU matches well with the Jones data. The peak at about 13 MeV (from the Li(p,n) reaction) is in both the simulation and the experimental data, and the slope upward below about 6 MeV is similar. Figure 4.7 includes lines indicating 25% above and below each Jones data point: for the most part, the MCNP data error bars stay within this range. There is a section from 6 to 11 MeV where the MCNP model did not register any counts. This result is reasonable due to the low statistics of the binning and could be more accurately modeled by increasing the number of particles in the run. This reaction is excellent for producing higher energy neutrons from lower energy. With 2 MeV deuterons, a peak around 13 MeV is created due to the ^{7}Li(d,n)^{8}Be reaction having a Q-value of 15 MeV.

The MCNP model produced a total neutron yield of 0.116x10^{9} n/μC/sr. Jones et

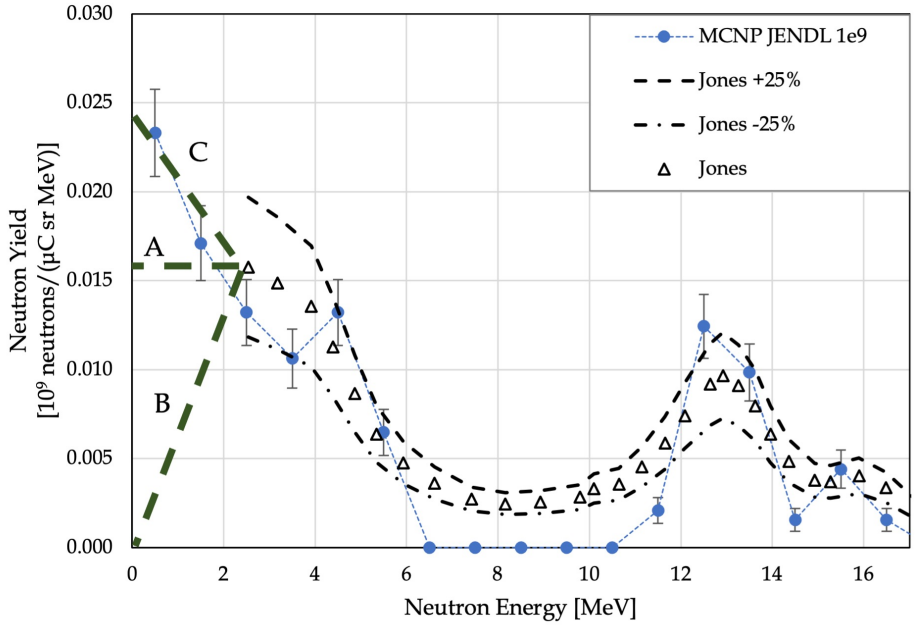

Figure 4.7. The ^{7}Li(d,n) reaction was modeled using both the JENDL/DEU-2020 library, and compared to the results of Jones et al. for 2 MeV incident deuterons [55].

al. report in Figure 5 of their article a value of 0.122x10^9 n/μC/sr, with a total uncertainty of 12-15%. Indeed, roughly interpolating their data in Figure 4.7 according to method A yields 0.124x10^9 n/μC/sr. The total neutron yield for Jones (reported using extrapolation method A) and MCNP agree to within 5%.

4.1.2.2 Deuterons on Beryllium

The ^{9}Be(d,n) reaction was modeled at incident particle energies of 2.6, 7, 8.8, and 16 MeV. Both the JENDL/DEU-2020 and TENDL-2019 libraries were used for the MCNP simulations for comparison, though TENDL greatly under-produced neutrons.

The 2.6 MeV run with the JENDL/DEU-2020 library compared well to the data from Meadows, et al. [56] (Figure 4.8). There is a peak in both the MCNP simulation and Meadows at around 1.75 MeV, though the coarse binning of the MCNP model adds some uncertainty. Above 2 MeV, most values match within a few percent. Using the TENDL library however, neither peak appears.

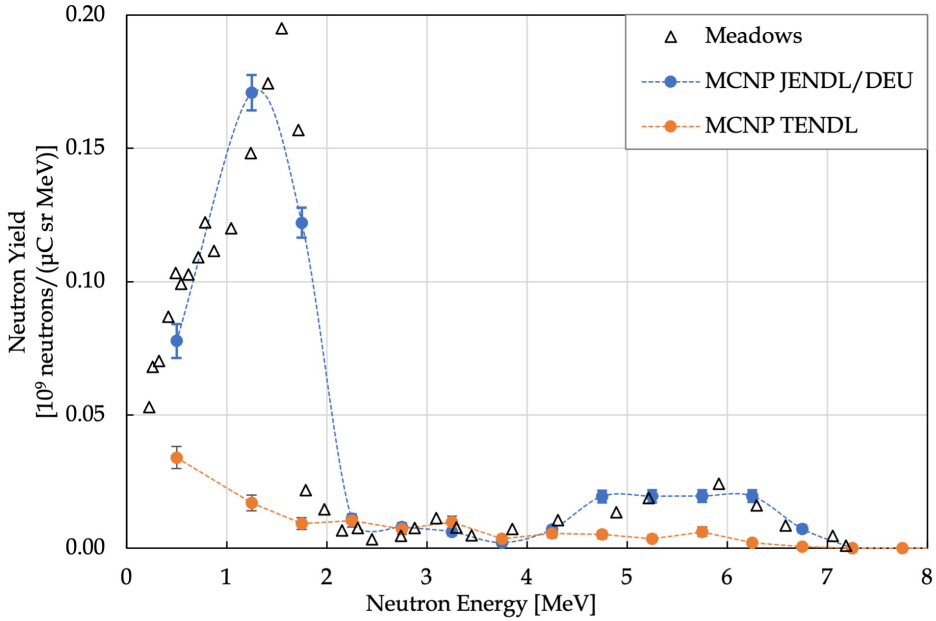

Figure 4.8. The ^{9}Be(d,n) reaction (E$_d$=2.6) was modeled using both the JENDL/DEU-2020 and TENDL-2019 libraries, and compared to the results of Meadows et al. [56].

The simulations using 7 and 8.8 MeV deuterons under-predicted neutron production below about E_n=4 MeV, indicating a shortcoming in the JENDL library at this neutron energy range. The TENDL library greatly under-predicts neutron yield across the entire energy range, in particular below 6 MeV. Indeed, this agrees with prior literature [75] and is a known problem. For each of the 7 and 8.8 MeV runs, the only setting changed was which cross section library was used. Smith et al. [76] also investigated 7 MeV deuterons on ^{7}Be but reported their values in arbitrary units, plotted with the secondary axis in Figure 4.9. The Meadows data has a local peak just below 1 MeV not seen in Smith. The binning is too large to see in MCNP. The 8.8 MeV run (see Figure 4.10) was similar to the 7 MeV run in that the JENDL library underproduced below 4 MeV

A study of 16 MeV deuterons bombarding a beryllium target was also conducted. Although this energy is outside the range of possibilities at NRL pulsed-power facili-

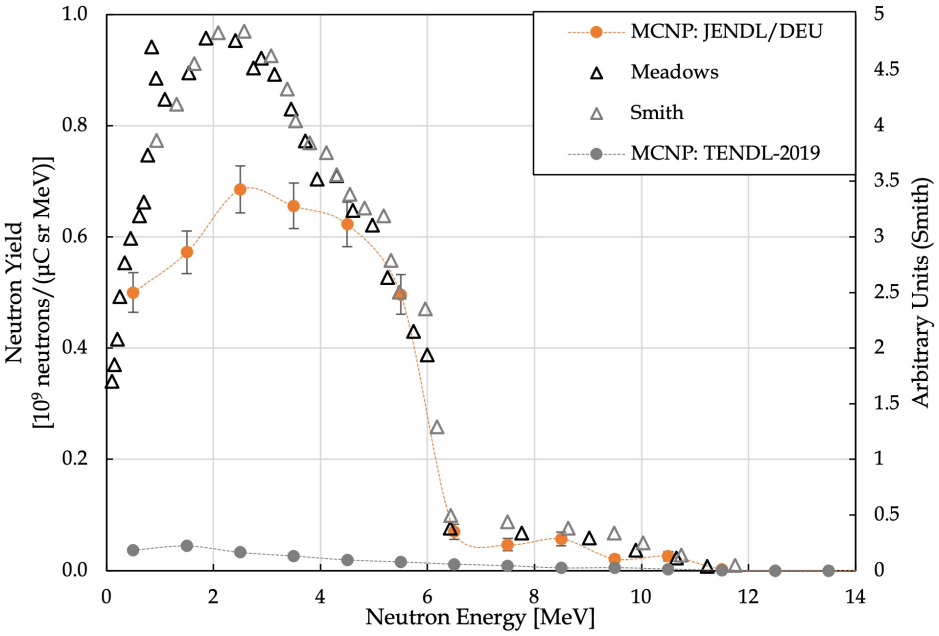

Figure 4.9. The ^{9}Be(d,n) reaction (E_d=7) was modeled using both the JENDL/DEU-2020 and TENDL-2019 libraries, and compared to the results of Meadows et al. [56] and Smith. et al. [76].

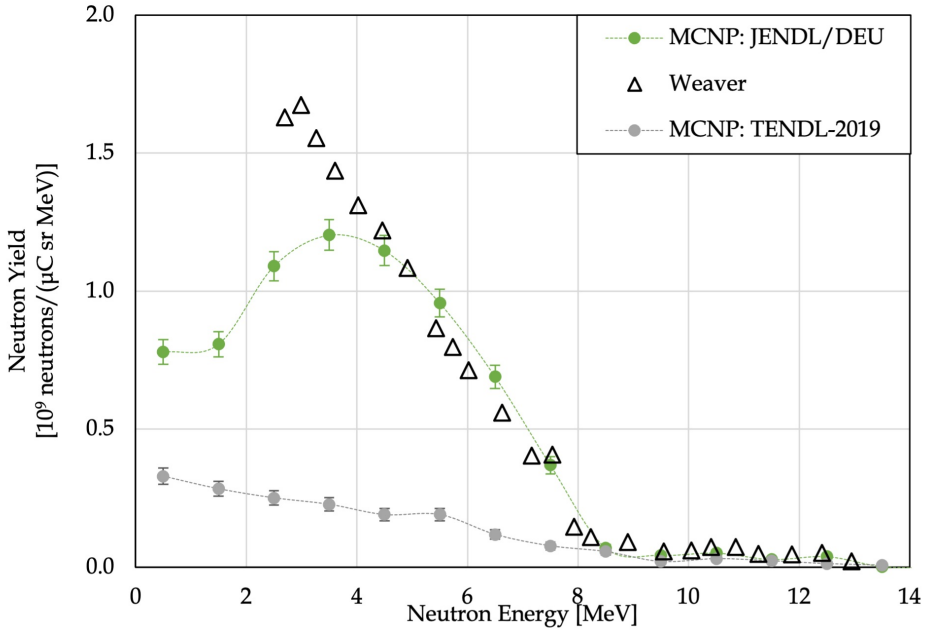

Figure 4.10. The ^{9}Be(d,n) reaction (E_d=8.8) was modeled using both the JENDL/DEU-2020 and TENDL-2019 libraries, and compared to the results of Weaver et al. [30].

ties, it proved useful due to the existence of multiple high quality measurements. The MCNP simulations were compared to several papers: measurements by Meulders et al. [50] and by Harrig et al. [49], and a hybrid breakup model developed by Morrell [9] that combines contributions from elastic and inelastic breakup. Meulders and Harrig themselves did not quite agree on the spectrum, but the JENDL library best matched the more recent Harrig data. TENDL again yielded significantly different results, creating a quarter of the neutron production seen in the other calculations and the measurements. The Morrell code modeled deuteron breakup by a combination of the Dancoff [37] and Serber [35] methods, focusing on deuteron energies above 16 MeV [9]. It underpredicts neutron production at 16 MeV, although not as much as TENDL.

The total neutron flux was also examined for the 2.6, 7, and 8.8 MeV runs, and summarized in Table 4.2. MCNP reported sum totals of the bins, which were then normalized by dividing by the bin sizes. The Meadows and Weaver totals were re-

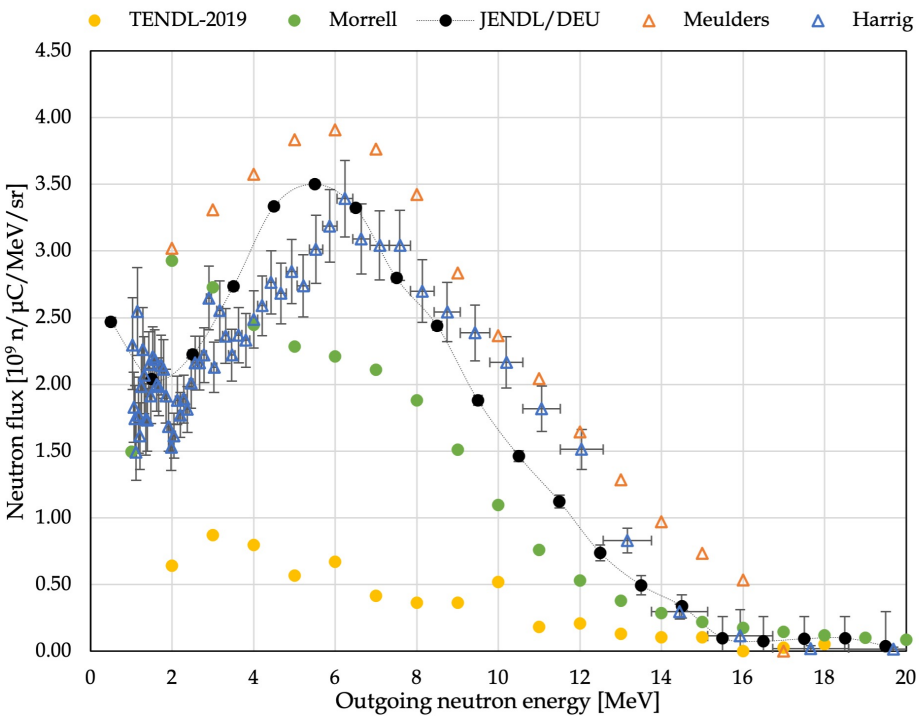

Figure 4.11. The ^{9}Be(d,n) reaction (E_d=16) was modeled using both the JENDL/DEU-2020 and TENDL-2019 libraries, and compared to the results of Meulders et al. [50] and by Harrig et al. [49] and a hybrid breakup model developed by Morrell [9].

ported in each, but their neutron spectra were also integrated for comparison. This integration was done using the right endpoint method, which is essentially the same as what MCNP reports. This adds some uncertainty to the integration, which was not quantified. Weaver only reported down to 2.5 MeV and used the same extrapolation method "A" as Jones, as previously outlined in section 4.1.2.1. The reported total production from the literature was used in the percent difference calculations. The difference in yield at 2.6 MeV is likely due to the coarseness of the bin sizes, combined with the sharp angle of the spectrum. The large difference in the 7 and 8.8 MeV runs are due to the discrepancy below 4 MeV.

Table 4.2. Total neutron production from the Be(d,n) reaction, in units of 10^9 n/μC/sr

E_d (MeV)	Meadows	Meadows Integrated	MCNP	% Difference
2.6	0.215	0.273	0.284 ± 4.2%	-32.2%
7.0	4.670	4.611	3.755 ± 1.9%	19.6%
	Weaver	**Weaver Integrated**		
8.8	9.116	9.347	7.2816 ±2.6 %	20.1%

4.1.2.3 Deuterons on Carbon-12

The C(d,n) reaction was modeled at 5 MeV, compared with a measurement by Tajiri, et al. [31]. The spectrum is shown in Figure 4.12. Like for the Be(d,n) reactions, the models underpredicted the neutron production from this reaction at lower energies, namely below 2.5 MeV. The JENDL MCNP model follows closely above 2.5 MeV, but underpredicts below that. The TENDL run only matches at about 3 MeV.

The total neutron flux was calculated for the JENDL run, summarized in Table 4.3. Tajiri et al. reported the total neutron flux but also found a curve fit equation for neutron production from 5 to 9 MeV incident deuterons. The results of this equation are also tabulated. The reported total flux was compared to the MCNP simulation, which only produced half the expected yield. This is also dependent on the confidence of the lower energies in the Tajiri data. The large difference is evident in the plot, greatly reducing the confidence of this reaction model's cross section data. Nonetheless, the total production is quite low compared to the lithium and beryllium reactions.

This production rate, lower than the lithium and beryllium reactions, is reasonable based on the cross section under 5 MeV, as shown in Figure 4.13. However, this decreases the likelihood of carbon being a good target material.

Table 4.3. Total neutron production from the C(d,n) reaction (E_d=5 MeV), in units of 10^9 n/μC/sr

Tajiri Reported	Tajiri Equation	MCNP Integrated	% Difference
0.440	0.441	0.220 ± 3.4%	50.0%

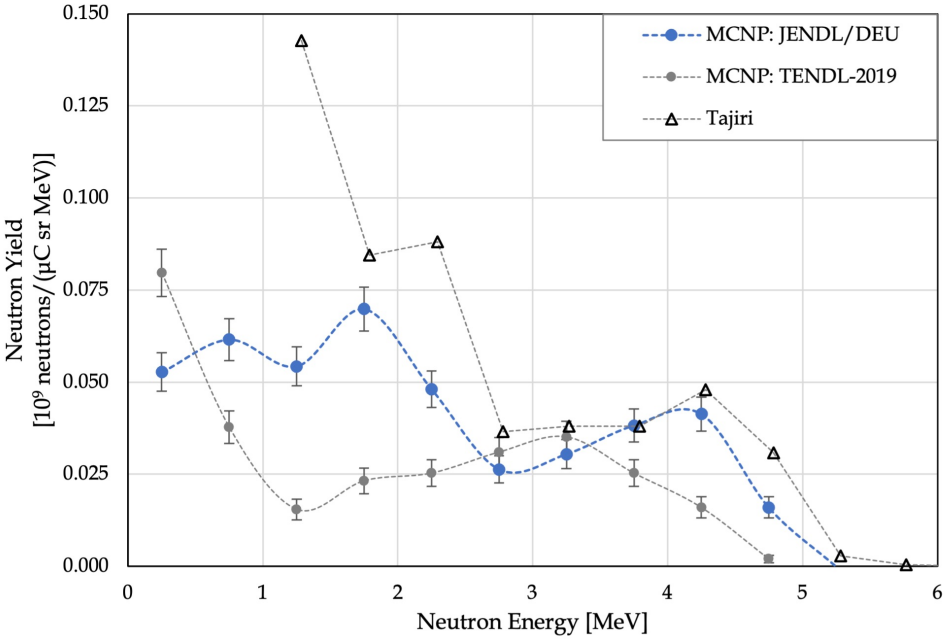

Figure 4.12. The ^{12}C(d,n) reaction (E_d=5 MeV) was modeled using both the JENDL/DEU and TENDL-2019 libraries, and compared to the results of Tajiri et al. [31].

4.1.2.4 Deuterons on Deuterated Polyethylene

The D(d,n) reaction is modeled with a potential target material, deuterated polyethylene. Both the D(d,n) and C(d,n) reaction are combined to consider the total neutron production that would occur using the material. The $D + D \longrightarrow {}^{3}_{2}He +$ n reaction has a Q value of 3.27 MeV. A 200 keV deuteron energy run was conducted but did not produce enough neutrons to be considered. With the incident energy of 2 MeV, neutron energies up to around 5 MeV can be expected. Figure 4.1.2.4 shows a peak at ∼4.75 MeV, within the 4.5-5 MeV bin. Since not all the Q value energy is imparted into the neutron, and the deuterons attenuate as they traverse the material,

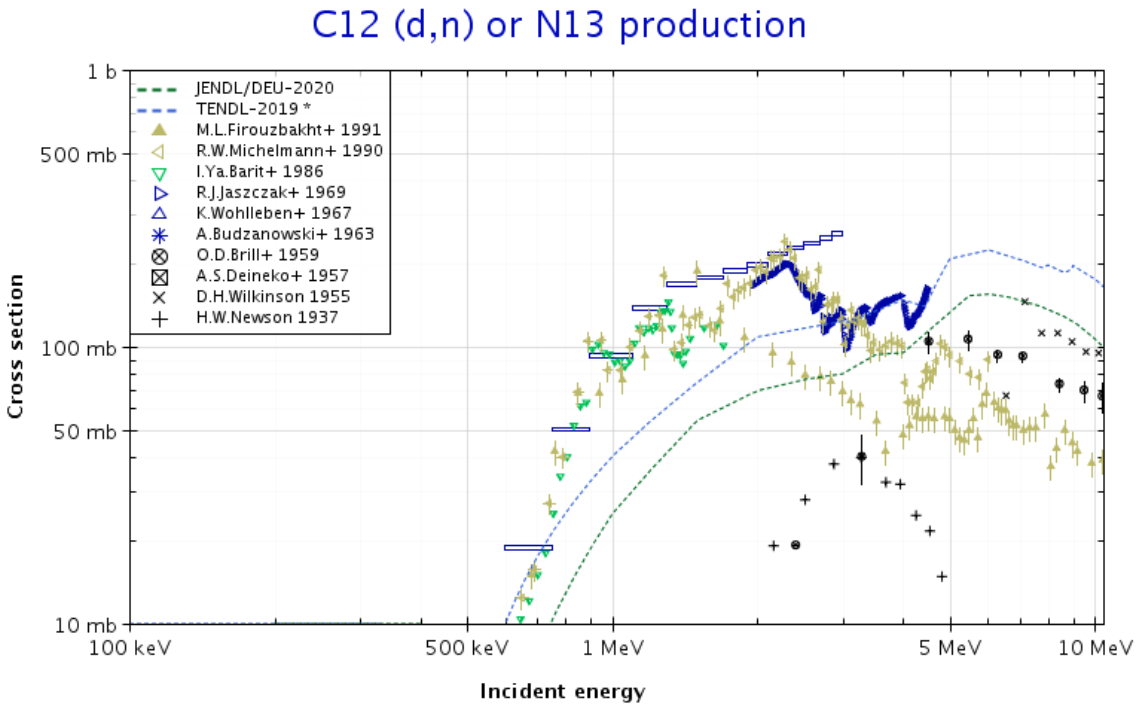

Figure 4.13. The ^{12}C(d,n) reaction cross section plot [74] according to JENDL/DEU peaks around 200 mb at ~5 MeV, though experimental reactions suggest this occurs as low as 2 MeV.

the peak just below 5 MeV is reasonable.

Here again the shortcomings of the TENDL library are evident,as this library does not produce the expected fusion neutron peak. This is odd considering the cross section used by the TENDL library as plotted in Figure 4.15 is consistent with experimental measurements and ENDF/VIII. As in the C(d,n) simulations, the CD_2 produces fewer neutrons than the lithium or beryllium reactions. One interesting possibility is the use of deuterated polyethylene on the back of the target to make use of deuterons that are too low in energy to produce neutrons via the other reactions.

4.2 Optimization Results

The multi-layered target was optimized to maximize total neutron flux in four scenarios: 2 MeV protons, 5 MeV protons, 2 MeV deuterons, and 5 MeV deuterons.

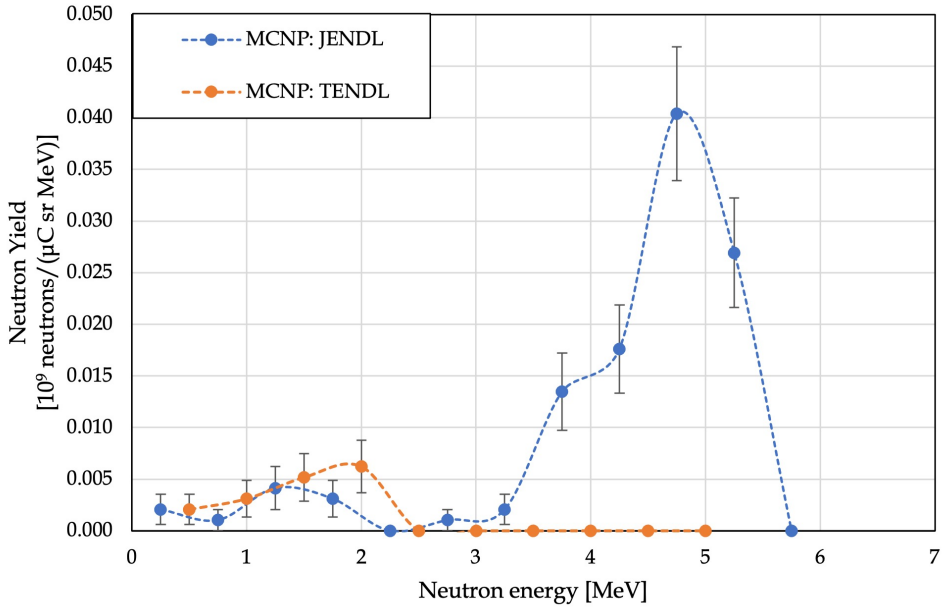

Figure 4.14. The CD_2(d,n) reaction (E_d=5 MeV) was modeled using both the ENDF/VIII and TENDL-2019 libraries.

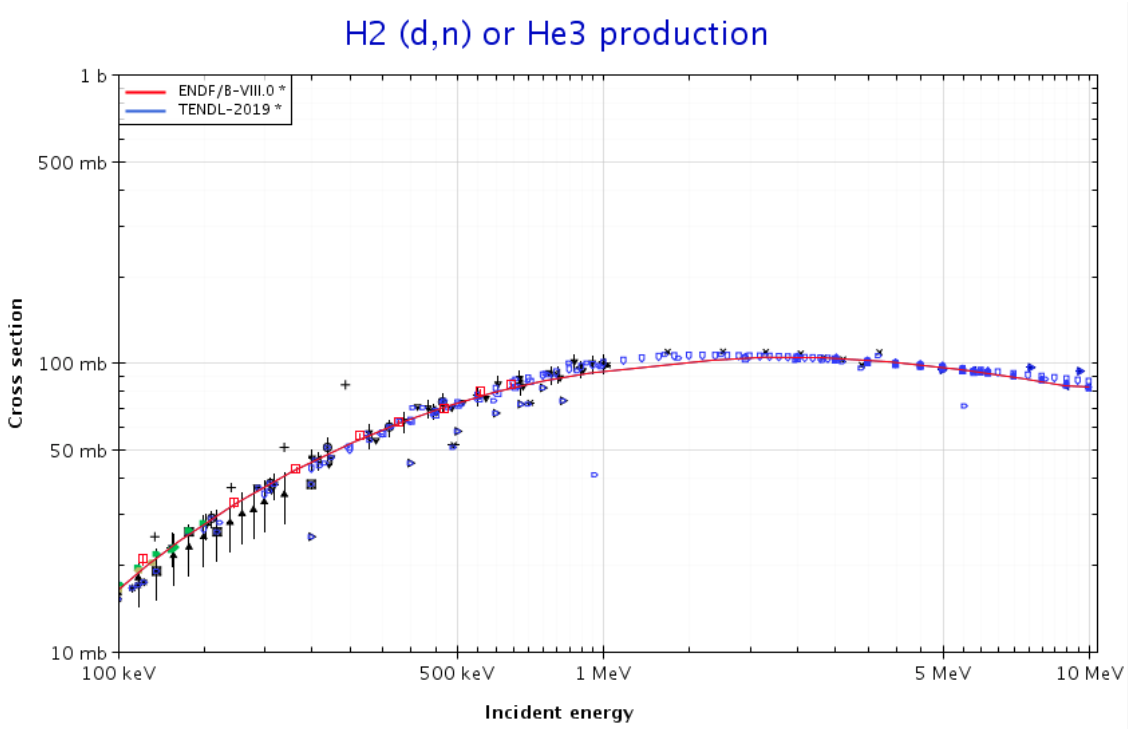

Figure 4.15. The D(d,n) reaction cross section plot [74] according to JENDL/DEU-2020 peaks around 200 mb at ∼5 MeV, though experimental reactions suggest this occurs as low as 2 MeV.

This section will discuss each run and its significance. The neutron spectrum of each is also discussed. A summary of the optimal targets are in Table 4.4, with total neutron production expected based on the assumed currents from Section 1.3.1.

4.2.1 2 MeV Protons

For 2 MeV protons, the best target consisted of only lithium with a thickness of at least 83 μm. The lowest percentage of the maximum thickness Dakota reported, as outlined in Section 3.3.2, was 52%. This is multiplied by the maximum depth of 2 MeV protons in lithium from Table 3.2 of 159.08 μm to get 83 μm. Only 52% of the total stopping distance is reasonable, as the protons are sufficiently slowed to reach below the threshold of the reaction.

Dakota does not know the protons can stop before reaching the next layer. Thus, there are several target compositions considered by Dakota in which the total thickness is much greater than the range of proton. As the thickness scan in Section 3.3.2 showed, additional thicknesses only very slightly decrease the forward detector counts, likely due to scattering and a small amount of neutron reactions. Given the statistical uncertainty in this work, the effects of extra target thickness are not a concern.

Figure 4.16 shows a plot of the total neutron production of each evaluation through which the Dakota software stepped. The best runs yielded a value of $0.035 \cdot 10^9$ n/μC/sr, but with a 20% statistical uncertainty. Methods of improving this simulation will

Table 4.4. Optimization layer thickness results

	Target composition (Thickness & Material)	n Production 10^9 n/μC/sr	Gamble II 10^{12} n/sr	Mercury 10^{12} n/sr
E_p = 2MeV	$>$ 83 μm Li	0.035	0.525	-
E_p = 5MeV	28 μm Be, $>$ 755 μm Li	0.927	-	2.78
E_d = 2MeV	15 μm Be, $>$ 50 μm Li	0.174	2.61	-
E_d = 5MeV	$>$ 150 μm Be	1.505	-	4.52

be discussed in Section 5.2. From these results, however, Dakota converged rather quickly to a straightforward solution.

The spectrum for this target is plotted in Figure 4.17. There is large statistical error due to too few *nps* in the run as a result of the low neutron production rate. MCNP repeatedly crashed beyond 10^8 particles due to an unresolved bug. (The CP2020 library seems to have been creating neutrons of negative energy, causing MCNP to crash. Investigation is ongoing.)It is thought to be a problem with the CP2020 library producing neutrons with negative energy. When compared to the 1.912 MeV validation results from Section 4.1.1.1, as in Figure 4.17, the spectrum looks generally plausible. The magnitude is similar for the reaction with just a 0.1-MeV incident particle energy increase, but slightly extended to form a wider peak. This flat region is also seen in the 2.5-MeV results in Figure 4.3, between the 1.912 MeV curve and beginning of the slope of the peak in the 2.5 MeV curve.

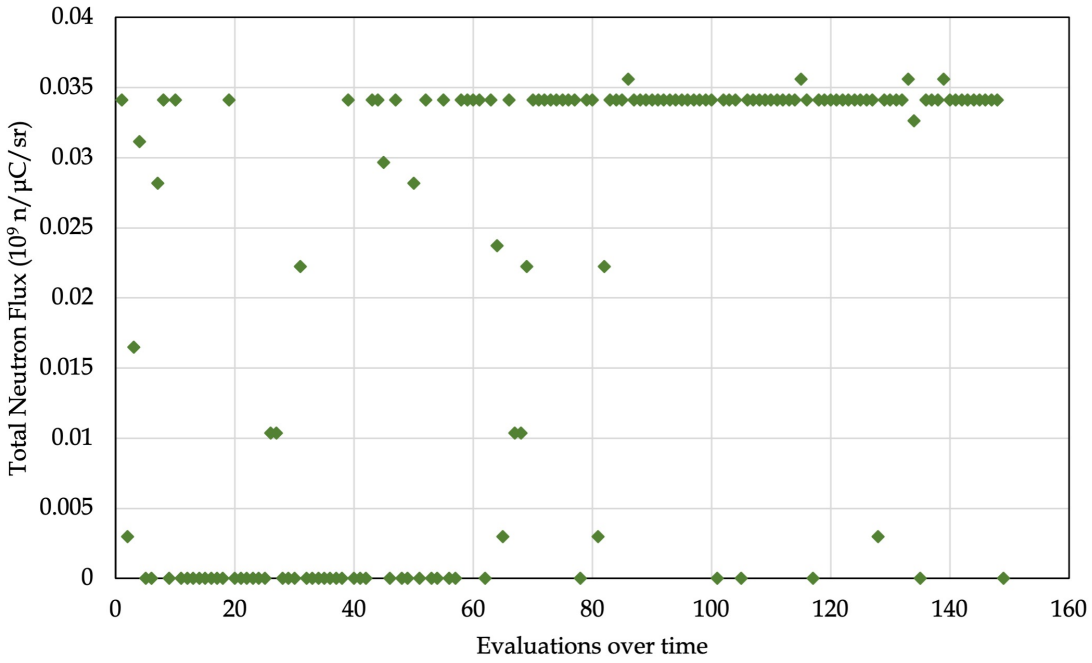

Figure 4.16. The Dakota evaluations for 2 MeV protons quickly reach a maximum of 0.035·10^9 n/μC/sr with a single 83 μm-thick lithium layer.

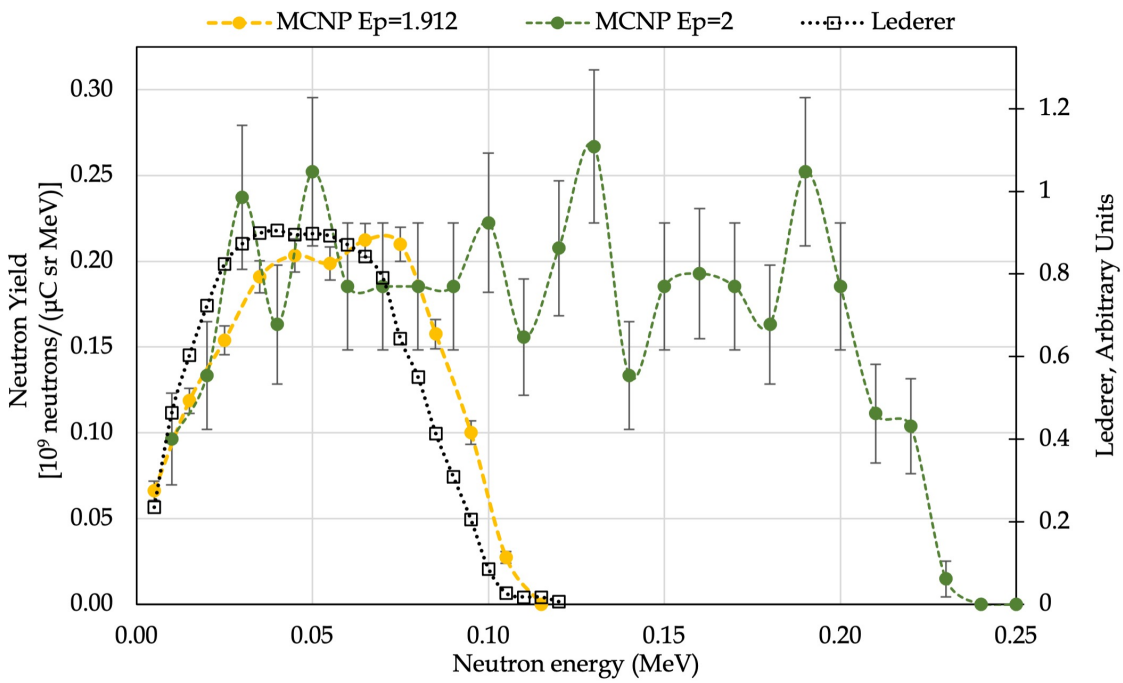

Figure 4.17. The optimized neutron spectrum from the 2 MeV proton run, along with the 1.912 MeV protons validation results.

4.2.2 5 MeV Protons

For the 5 MeV proton run, the optimized target was 28 μm of Be, followed by at least 755 μm of Li, for a total neutron production of $0.927{\cdot}10^9$ n/μC/sr, $\pm$9%. However, an all-lithium target produced just 2% fewer neutrons, for a total of $0.905{\cdot}10^9$ n/μC/sr, $\pm$9%. Since these two are within the statistical uncertainty of the other, they would be considered the same in terms of total production. However, the ^{9}Be(p,n) cross section is slightly higher at 5 MeV, indicating an expected slight increase in total production for the optimal configuration proposed by Dakota. Nonetheless, it may very well be that this small percentage does not justify adding a material like beryllium, which can pose significant safety risks.The evaluations are plotted in Figure 4.18, which shows a good convergence, though the average plateaus at about 300 evaluations. Note also the banding that occurs at about the $0.4{\cdot}10^9$ n/μC/sr level. This is the pure beryllium target total output.

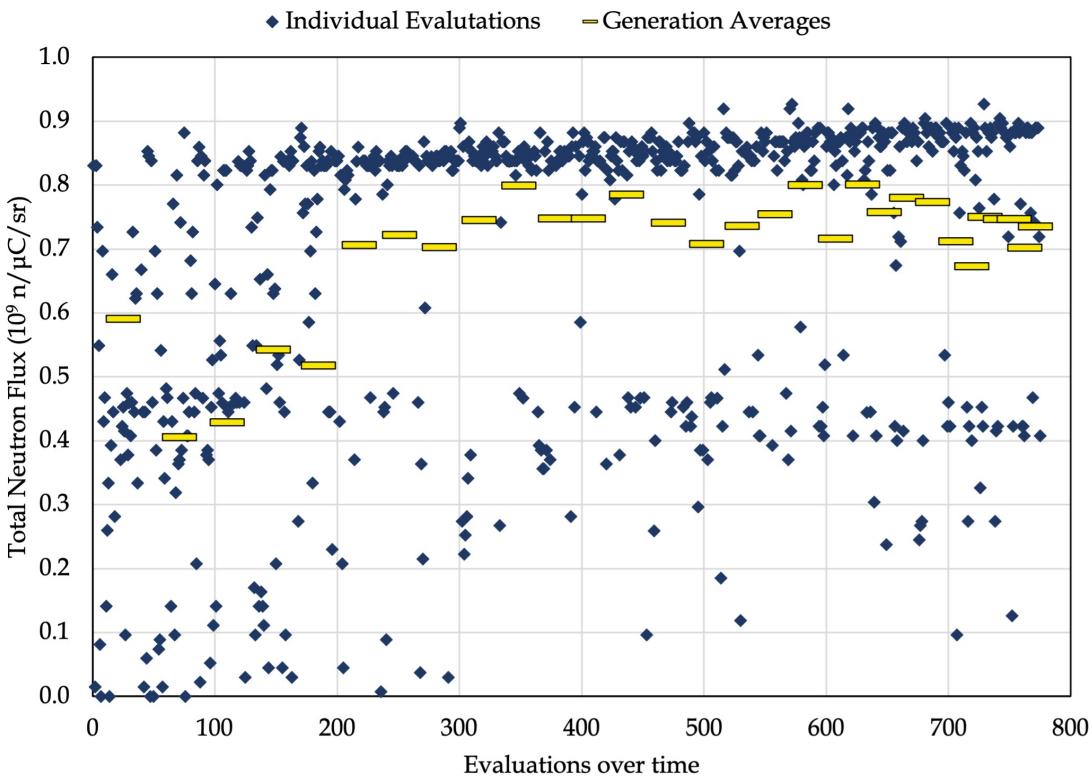

Figure 4.18. The optimized target for 5 MeV protons is 28 μm of Be, followed by at least 755 μm of Li. The average values of each generation are also plotted, and shown to plateau at about 300 evaluations, though the upper level convergence does not happen until about 775 evaluations.

The outgoing neutron spectrum is plotted in Figure 4.19. A contribution of neutrons from each layer is plotted in Figure 4.20. The first peak at about E_n=0.6 MeV is consistent with the E_p=2.5 MeV reaction in Figure 4.3. The peak at ~E_n=3 MeV is consistent with that of Figure 4.6. The peak at ~E_n=4.3 MeV was not seen in the validation, since the Li(p,n) reaction was only evaluated at E_p=2 MeV, below higher reaction thresholds. Looking at these threshold and Q-values however, the 4.3-MeV peak is likely not from the cross section library. THe library used, CP2020, only consideres deuterons on lithium up to 3 MeV. It is likely MCNP's model physics (MPHYS) settings – which are not optimized for sub-100 MeV ions – is creating these. In turning this setting off, the peak disappeared, but the spectrum was slightly different. The rest of the MCNP simulations were done with model physics on, but since

the cross section libraries covered the particle energy ranges, it is unlikely this had additional impact. Further investigation was not completed.

Also considered for this reaction was the distribution of a target with a beryllium first layer and lithium second layer. Each evaluation that met these two criteria (including those that had "zero" thickness, i.e., only beryllium or only lithium as well), was plotted in Figure 4.21. If a material was used on two consecutive layers, such as "Be-Li-Li," then these layer thicknesses were added. Note the different scales of the axes (beryllium's maximum thickness was less than lithium due to the higher stopping power). Dakota tended to band and leave gaps in the phase space sampled. Two MCNP parameter studies (p-study) [77] were done running through a more uniform

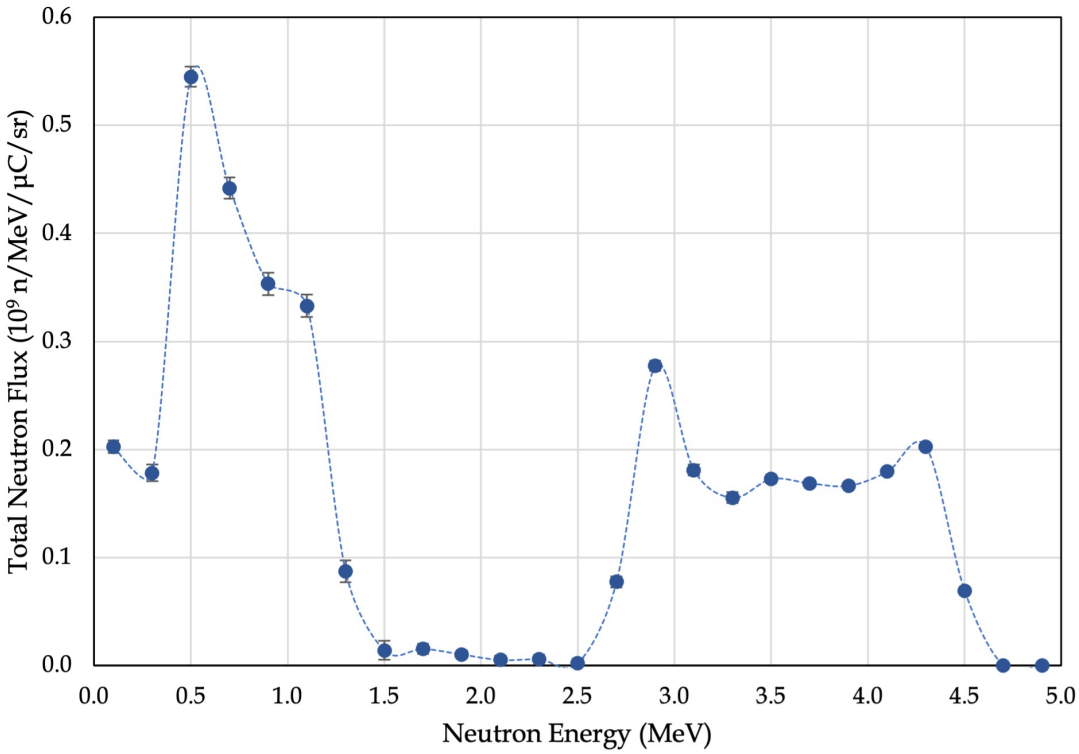

Figure 4.19. The spectrum from the 5 MeV protons on beryllium and lithium target shows the peaks from the individual reactions, but also the unknown production above 3 MeV, likely due to model physics. This MCNP setting was turned on for this run, and the cross section library used only considered proton energies up to 3 MeV. There are no Q values for reactions that produce the peak at 4.2 MeV.

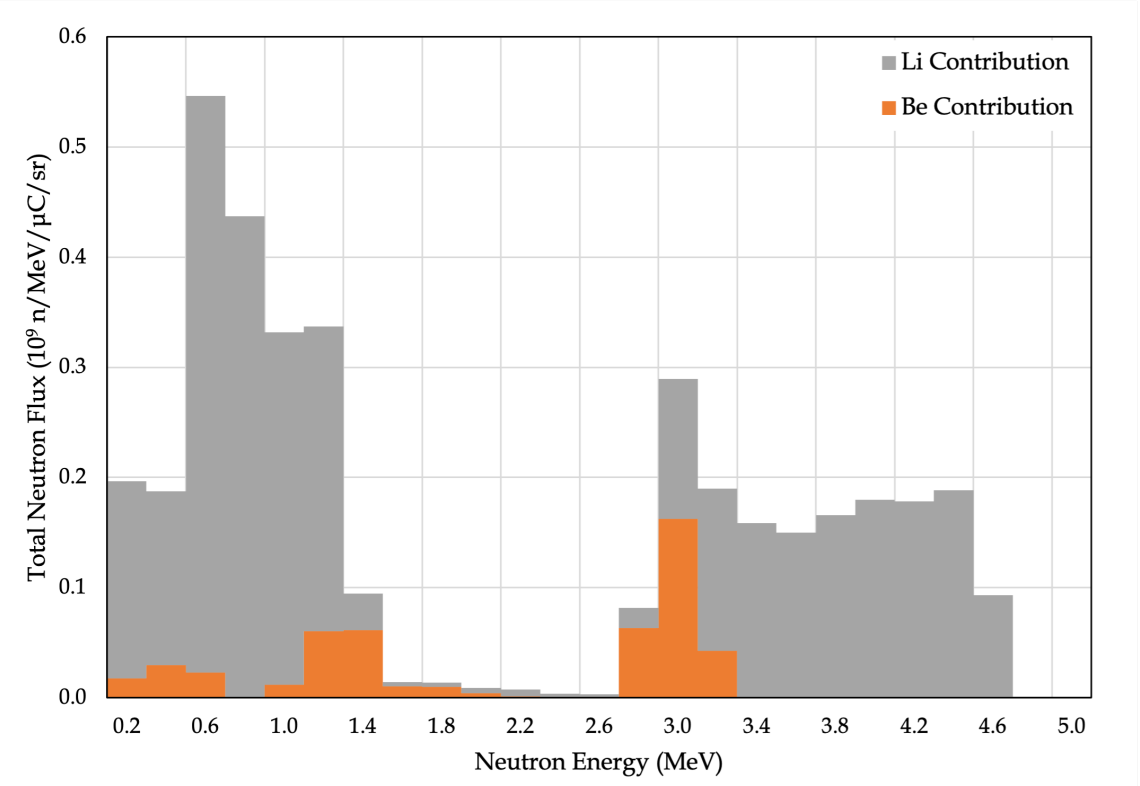

Figure 4.20. The lithium layer for the optimized 5 MeV proton target produced the vast majority of the neutrons.

set of points for the 5 MeV protons. The second was done to fill in gaps the first one left. These are combined in Figure 4.22. The two show interesting banding, with the highest production appearing at beryllium thicknesses of ~0.0025 cm, ~0.0075 cm, and ~0.014 cm. An explanation for this is the statistical variance due to the Monte Carlo method. Both sets had uncertainties of ~9-10% for *nps*=1e6, which easily encompasses the variance. A key feature, however, is that the points where the beryllium thickness is 0, the total neutron production dips below $1.6 \cdot 10^9$ n/μC/sr. While just at the edge of 10% variance, it does indicate that some beryllium at higher proton energies does increase neutron production as expected based on the cross section at 5 MeV.

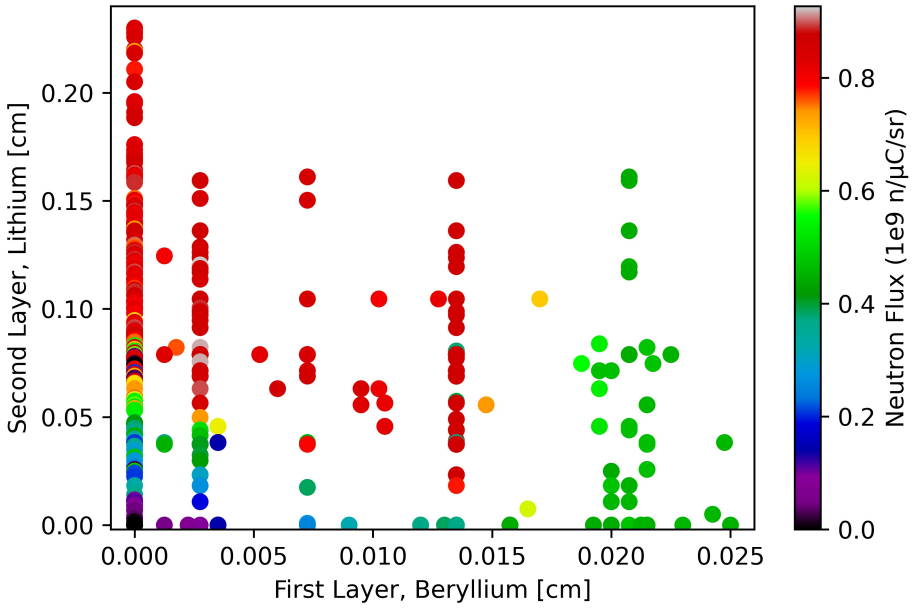

Figure 4.21. For the 5 MeV protons run, the evaluations of lithium and beryllium layers show the parameter space and gaps in thicknesses.

4.2.3 2 MeV Deuterons

For the 2 MeV deuteron run, the optimized target was 15 μm of Be, followed by at least 50 μm of Li, for a total neutron production of $0.174{\cdot}10^9$ n/μC/sr, $\pm$7%. The evaluations converge much more prominently in Figure 4.23. Some zero-value evaluations were removed due to a timeout bug in the code.

The neutron spectrum for this optimized target is plotted in Figure 4.24. The peak at $\sim$1 MeV is consistent with the peak in the Be(d,n) validation simulations for 2.6 MeV deuterons (Figure 4.8), and with the rise as the neutron energy goes to zero in the E_d=2 MeV Li(d,n) reaction of Figure 4.7. The height of this peak also indicates that most of the deuterons are interacting in the first layer of beryllium. The slight peaks at $\sim$5 MeV and $\sim$12.5 MeV are also consistent with the E_d=2 MeV Li(d,n) reaction of Figure 4.7.

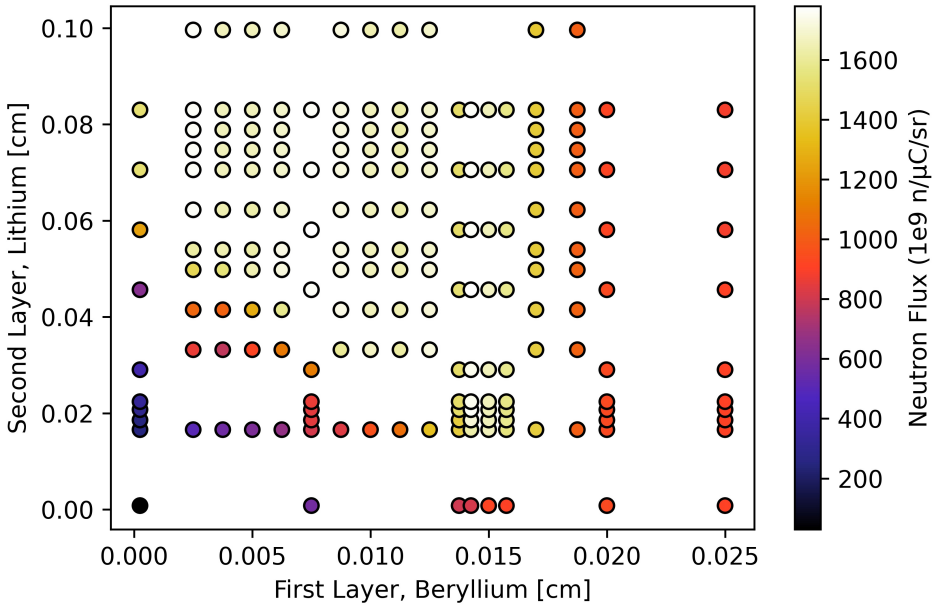

Figure 4.22. The MCNP p-studies for 5 MeV protons show areas of high neutron production, but also shows the variance between the two studies due to uncertainty. The statistical uncertainty reported by MCNP was just under 10%.

4.2.4 5 MeV Deuterons

Finally, the optimization results suggest neutrons are best produced from 5 MeV deuteron using an all-beryllium, >150-μm-thick target. This beam produced the most of all four, with $1.505{\cdot}10^9$ n/μC/sr, $\pm$7%. Figure 4.25 shows the convergence in about 160 evaluations.

There is no contribution from a lithium backing as in the 2 MeV run. This seems to make sense as the beryllium cross section of the reactions appears to be higher than that of lithium (see Figure 4.26), but this raises a question as to the validity of the 2 MeV run. One reason this difference may occur is the angular distribution of the outgoing neutrons. Perhaps the low energy deuterons in the Be(d,n) reaction produce neutrons at angles greater than 30° (as in the Li(p,n) reaction, Section 4.1), but do not with the Li(d,n). This would make the Li(d,n) reaction more productive for forward

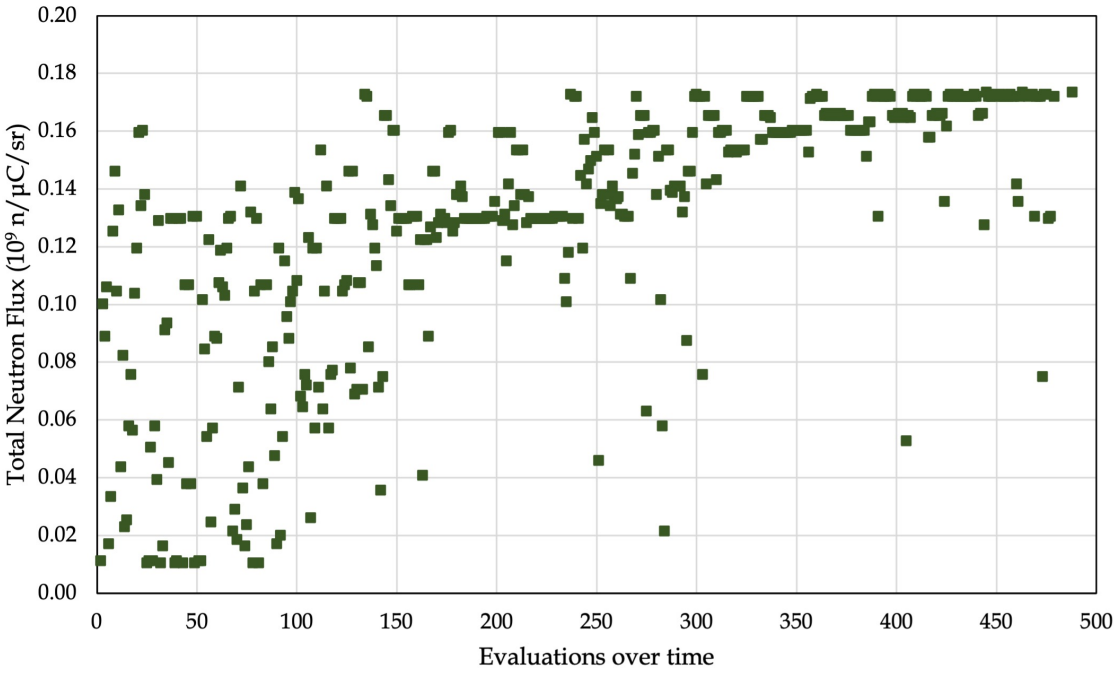

Figure 4.23. The 2 MeV deuteron optimization evaluations clearly converge on a target composition of 15 μm of Be, followed by at least 50 μm of Li.

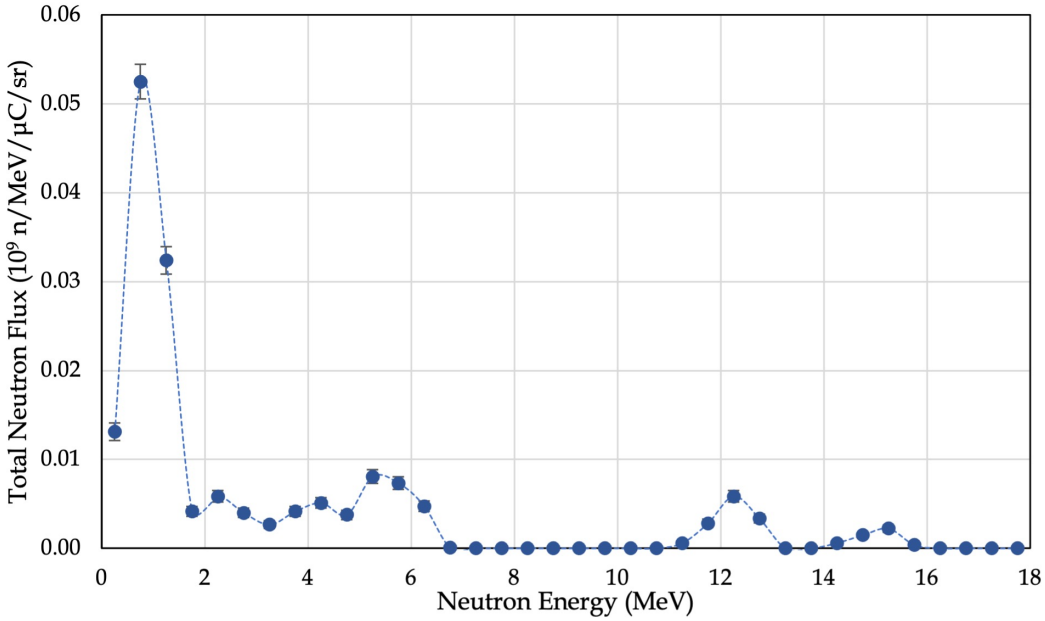

Figure 4.24. The outgoing neutron spectrum for the E_d=2 MeV optimized target agrees with the MCNP validation results in Section 4.1.2.

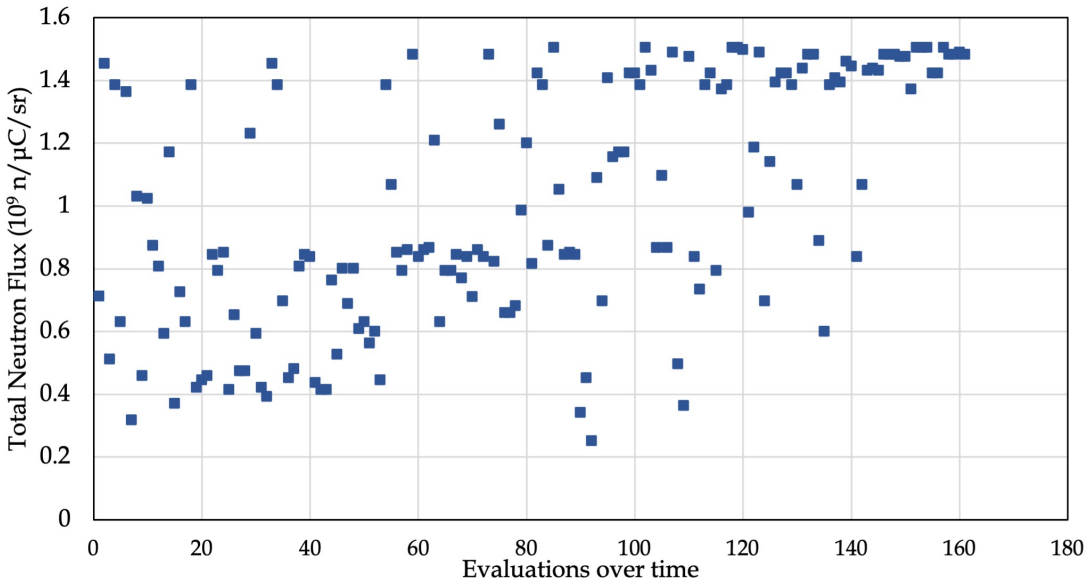

Figure 4.25. The 5 MeV deuteron optimization evaluations clearly converge on a target composition of at least 150-μm-thick beryllium.

neutrons, hence the inclusion in the 2 MeV run. But even the 5 MeV deuterons deposit energy down below 2 MeV, so this still does not explain the aforementioned results. Further investigation was not conducted.

This neutron spectrum from 5 MeV deuterons looks like a combination of the 2.6- and 7-MeV deuterons on beryllium validation runs, but with an extra feature between 7 and 8 MeV. The E_d=2.6 MeV Be(d,n) reaction has a peak at neutron energies about 1.5 MeV, and some production at 5-6 MeV (Figure 4.8). The E_d=7 MeV Be(d,n) reaction has a wide peak over neutron energies from 2-6 MeV, and some production at 7-9 MeV(Figure 4.9). Since the wide first peak in the Figure 4.27 plot drops off at 4 MeV, the 4-6 MeV production and the double magnitude in the E_d=7 MeV reaction is due to the higher deuteron energy. The neutron production of the E_n=7-9 MeV range is not necessarily then dependent on the 7 MeV deuteron energy: it could come from deuterons less than 5 MeV, appearing on the 7 MeV plot from deuterons that had been depositing energy down below 5 MeV.

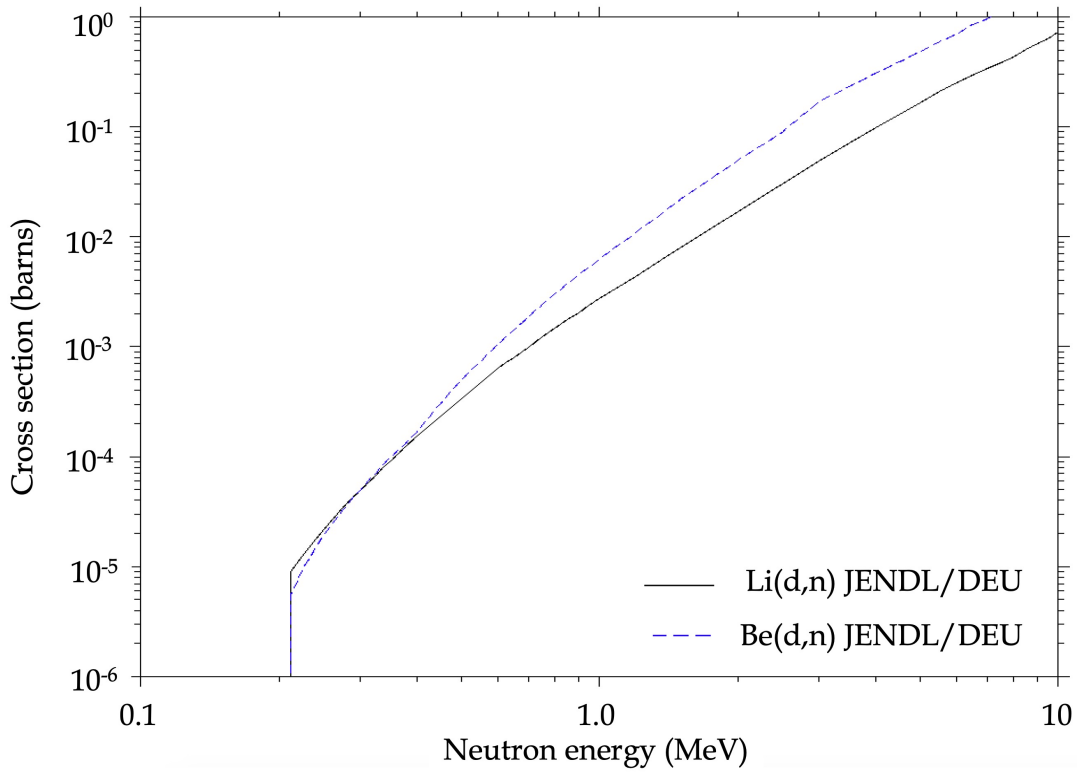

Figure 4.26. The cross section of the Li(d,n) and Be(d,n) reactions, as plotted by MCNP's *mcplot* and defined by reaction number MT=4, shows the beryllium reaction as higher than lithium down to about 0.3 MeV

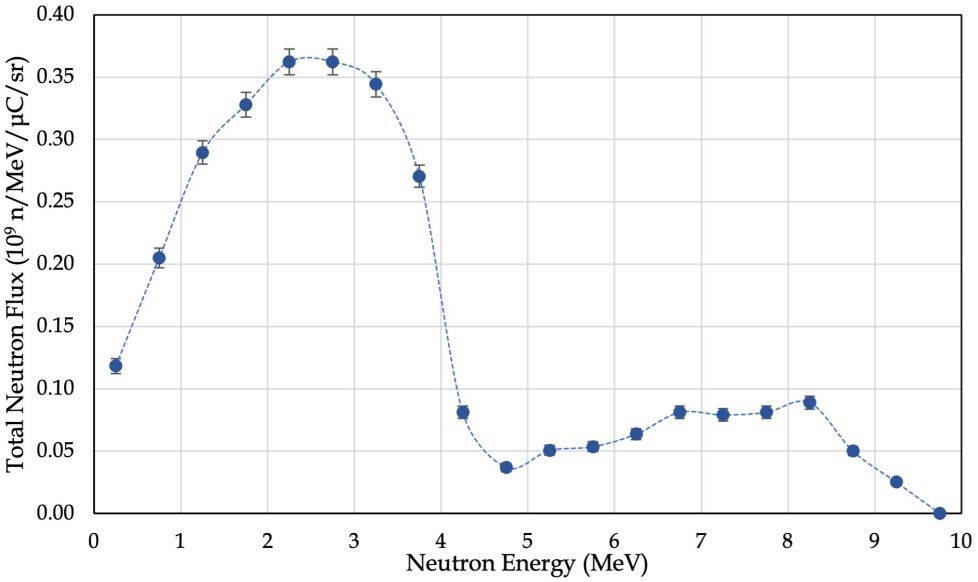

Figure 4.27. The outgoing neutron spectrum for the E_d=5 MeV optimized target agrees with the MCNP validation results in Section 4.1.2.

V. Conclusions

5.1 Summary

There is a need for neutron sources for national security and other fields of research. NRL is interested in using the ions from their pulsed-power generators to produce neutron environments. This research explored what target materials best leveraged NRL's pulsed-power facilities to produce neutrons. Various reactions were considered and optimizations were run to determine the material orders and layer thicknesses that produced the most neutrons in the forward direction. NRL's facilities produce 2 MeV (from Gamble II) and 5 MeV (from Mercury) protons and deuterons.

The materials chosen for this work were lithium, beryllium, carbon, and deuterium in the form of deuterated polyethylene (CD_2). These were chosen for their common usage in other neutron production facilities, availability of experimental measurements in literature that could be used for model validation, and high cross section for low energy neutron production. Other materials identified but not used in optimization were tritium, oxygen, vanadium, tantalum, and titanium. Tritium was not considered due to cost and safety concerns, and the others because the cross sections were low below 5 MeV. The expectation was that due to different characteristics of the materials – cross sections and outgoing neutron angular distribution – that there may be a best combination to most effectively produce neutrons. The model was implemented using MCNP to simulate the reactions and determine the total and energy-dependent neutron production. The objective of finding the best material combinations was accomplished through a two-step process. First, it was deemed necessary to validate models for each reaction against literature.Second, the actual optimization for each of the four scenarios was developed. The optimization

was implemented in a code suite to enable future extension to other materials, target geometries, and beam spectra.

The ^{7}Li(p,n) reaction was modeled with the the CP2020 cross section library at proton energies of 1.912 and 2.52 MeV. The 1.912 MeV reaction matched the general shape of the spectrum from literature – which used arbitrary units for the neutron production – but was shifted about 10% toward higher energies (Figure 4.1). The 2.52 MeV reaction was shifted less than ∼5% toward the lower energies, but matched the magnitude of the literature well (Figure 4.3). The ^{9}Be(p,n) was evaluated at proton energies of 3.7 and 5 MeV using the ENDF/VIII-B library. The 3.7 MeV reaction matched within about 5% to the two peaks in the literature, but had an additional peak between the two (Figure 4.5). This created an additional 45% total neutron production. The 5 MeV results were slightly better, but one peak was significantly shifted higher by half an MeV (Figure 4.6). The total neutron production in the forward direction was within a few percent of the literature.

The ^{7}Li(d,n) reaction was only modeled at a deuteron energy of 2 MeV due to the limited literature. The JENDL/DEU-2020 library matched the literature fairly well, generally within 25% (Figure 4.7), and the total neutron production agreed with literature within 5%. The ^{9}Be(d,n) was evaluated at deuteron energies of 2.6, 7, 8.8, and 16 MeV using the JENDL and TENDL libraries. The 2.6 MeV shape was modeled fairly well (Figure 4.8), but was about 30% off the total neutron production reported by the literature. The 7 and 8.8 MeV runs using the JENDL library underpredicted neutron production below 4 MeV (Figures 4.9 and 4.10), both about 20% off the total neutron production. The 16 MeV was close to the most recent literature, Harrig, but about 10% smaller than the 1972 Meulders data (Figure 4.11). In each of these, the TENDL library greatly under performed and is not recommended for use in this specific case. The ^{12}C(d,n) reaction was evaluated at 5 MeV, also with the JENDL

library. It underpredicted neutron production below 2.5 MeV and the total neutron by 50% (Figure 4.12). Literature was not found to compare the neutron spectrum from 2 MeV deuterons on deuterated polyethylene, with the intent of combining the ^{12}C(d,n) and D(d,n) reactions. A 200 keV deuteron energy run was conducted but did not produce enough neutrons to be statistically considered. The MCNP results for the CD_2 model (Figure 4.14) showed a peak at about 4.8 MeV. Since the Q-value for the D+D reaction is 3.27 MeV, the location of this peak is reasonable for 2 MeV protons. The neutron production was about an order of magnitude lower than that of beryllium and lithium, so it was unlikely to be a good target. The low forward production at 200 keV did not bode well for the idea of using CD_2 as a backing to react with deuterons that had deposited their energy in the target, going below any reaction thresholds. Also simulated was the V(p,n) reaction at proton energy of 5 MeV, but the low production rate and lack of literature prevented it from being considered in this research. The MCNP validation process showed that while some reactions were modeled very well, there exists gaps between MCNP simulations using cross section libraries and physical experiments in literature.

The optimization runs yielded different preliminary targets for each of the four scenarios, summarized in Table 4.4. The 2-MeV proton matched intuition as the cross section of the ^{9}Be(p,n) drops precipitously at 2.1 MeV, while the ^{7}Li(p,n) cross section holds at over 250 mb from 2 MeV down to the threshold at 1.88 MeV. This target was calculated to yield 0.035 10^{9} n/μC/sr, or 0.525 10^{12} n/sr from Gamble II. For the 5 MeV proton run, the ^{7}Li(p,n) cross section is generally higher than the ^{9}Be(p,n) reaction under about 8 MeV, at least for the ENDF/B-VIII.0 library used in the simulation. However, the optimization suggests that a thin slice of beryllium in front of a thick lithium target has about the same neutron production as an all-lithium target. The statistical uncertainty of the MCNP simulations was around 9%,

and the difference between the two target designs was about 2%. Since the beryllium layer is so thin, the 9% variation is reasonable to compare to an all-lithium target, particularly since the cross sections of each are within 10% around a deuteron energy of 5 MeV. This target was calculated to yield 0.927 10^9 n/μC/sr, or 2.78 10^{12} n/sr from Mercury.

This reaction also revealed a potential flaw in the MCNP model and using some libraries. In this 5 MeV proton case, the CP2020 library was used, which only goes up to 3 MeV protons on ^{7}Li. The extra area in the neutron spectrum in Figure 4.19 was found to likely be from the model physics. When turning the model physics off, extra neutron production appeared, but it is unclear how MCNP handles being forced to contend with energies above the maximum in a cross section library as the results conflict with the manual guidance. All of the optimization runs were done with model physics on, and these were not checked to see how they behaved with the option off. For instance, the peak in the 3.7 MeV protons on beryllium: was it caused by the model physics or a peculiarity in the cross section library?

The 2 MeV deuteron run had the smaller convergence limit of 1% and increased initial population of 50. These changes increased the precision and therefore confidence over previous runs. According to the cross section plots of the ^{7}Li(d,n) and ^{9}Be(d,n) reactions, ^{9}Be generally dominates. It could be that the angular distribution of the outgoing neutrons differ, and so while interaction with beryllium is more likely, interactions with lithium actually produce more forward neutrons. More investigation would be needed to back up this supposition however, as will be discussed in the next section. This target was calculated to yield 0.174 10^9 n/μC/sr, or 2.61 10^{12} n/sr from Gamble II.

The 5 MeV deuteron run had a 10% convergence limit and an initial population of only 25 for the Dakota input file. These parameters can restrict the number of

samples Dakota makes, increasing the likelihood of finding a local maximum, rather than a global one. This tendency may explain the lack of the lithium back layer as in the 2 MeV run. This target was calculated to yield 1.505 10^9 n/μC/sr, or 4.52 10^{12} n/sr from Mercury.

The 2-MeV deuteron reactions had a production rate 4 times that of 2 MeV protons, and 5 MeV deuterons had nearly double the production of 5 MeV protons.

This work investigated the process of designing an optimized target for neutron production with pulsed-power generators. It took a multi-layered target approach not greatly explored in current literature. MCNP models of reactions at various energies were compared to experiments in literature, revealing shortcomings in current cross section libraries and the importance of these libraries. An optimization approach was developed to combine multiple materials for four scenarios. This can be taken further to additional materials, energies, libraries, and refined techniques to provide a greater understanding of the merits of multi-layered versus single material targets. This lays the foundation for additional objective functions to be explored based on need, such as neutron energy spectra, angular distribution, and uniformity. Neutron production from pulsed power is a promising alternative to other more costly and infrequent sources.

5.2 Future Work

Finishing the design and fabrication of a neutron-producing pulsed-power target for NRL is an endeavor that exceeds the ability of a single Master's student in 18 months. While a good step forward was taken, far more can be done. This section will step through what is lacking in the current work – the validation and initial optimization – and suggestions for how to take it further.

There were many gaps in the validation studies. Of the materials studied, vali-

dating the reaction cross section models at additional energies would be beneficial, including 5 MeV protons on lithium and 5 MeV deuterons on beryllium, lithium, and CD_2. Additional materials can also be considered to increase the optimization space. Only two materials for proton reactions greatly limited the potential material combinations, though layer thicknesses added complexity. Oxygen, vanadium, tritium, tantalum, and titanium are among those identified of future interest to the optimization. The higher Z materials have significant cross sections at energies above 5 MeV however, and may not be available for use within the current NRL facilities.

With the large discrepancies in some of the validation runs, understanding what reactions the libraries considered and modeled, as well as their outgoing energy and angular distribution, would provide insight into how they shape the MCNP results. In addition, going through each result to look at the impact of model physics — if they were used or not — would build confidence in the libraries and current results. If the model physics did have an impact on neutron production, rerunning the validations and optimizations would focus the results on what only the libraries produce. A far more in-depth verification and validation study is recommended.

Additionally, other types of reactions could be considered. Gamma ray production would be useful to know for a particular target. Neutron reactions within the targets may impact how many escape the target. Secondary reactions, particularly with deuteron fusion reactions, may change the neutron production or spectrum.

An additional feature of the neutron production, which was not an objective of this research, is that of the outgoing neutron spectrum. While spectra were plotted for the results discussed here, an additional or alternative objective function to be optimized would be a specific single energy peak or specific neutron spectrum shape. The maximization of production would be set as a lower priority, and the different materials would provide an excellent palette to paint a particular picture. This could

be done using the same SOGA method with the spectrum as the only objective, or through a similar multi-objective genetic algorithm (MOGA), where the spectrum and production are optimized.

Sources of uncertainty varied greatly in this work. While most of the validation runs showed the general shape with a statistical uncertainty of 5-10% for each bin, the optimization runs had much higher uncertainties. To decrease the uncertainty, number of particles run would increase as would the runtime. The optimizations and validations were run on a single node. Running on more nodes would greatly decrease the run time and/or allow for more particles to be run. Since the optimization convergence criteria can be set to 1% or similar, the MCNP models could also be run to produce a statistical uncertainty of less than that precision. To cite a specific example, the 2 MeV proton run had a large statistical error, only $\sim$160 evaluations, and a 10% convergence. The 2 MeV deuteron run was initially done with these same settings, and initially missed what became the final result. While a different result is unlikely based on the cross sections, things like this can easily be missed without optimal settings. The 5 MeV deuteron run likewise had about 160 evaluations and should be investigated further. The current optimization runs left large gaps in the parameter space, as in Figure 4.21. Increased processing power would enable a larger initial population and more sampling. More settings, such as crossovers or mutation, could be tweaked and explored to get a more complete picture of the parameter space.

An MCNP variance reduction technique, which could also provide more information about the out-going neutrons, would be to use the *cn* tally cosine card. This could determine the angle of the neutrons as they left the back of the rear-most layer, binning over certain angles. This card would eliminate the need for the large boundary cylinder and may speed up the runs.

When the MCNP parameter study was conducted on the 5 MeV proton run,

there was still considerable variation between neighboring points (Figure 4.22). The lighter (higher neutron production) points vary fairly obviously from one thickness to another, an example of the statistical uncertainty within MCNP. The iterative p-study scans did not take much longer than the Dakota optimization, which had a large amount of bunching and banding. Granted, this case was with two materials, but with three or even four layers, consideration of this enumerative approach may be worthwhile. This could also be done with Dakota with more materials.

The code suite could also be improved. Currently the Dakota software does not correlate which material is assigned to the layer thickness. They are independent of each other: if a first layer value of a contributes to a higher neutron production, Dakota does not know that it was also a layer of material b at thickness a which is producing more neutrons. Instead, the number a shows up frequently and Dakota continues to choose that value at the expense of others. This can be seen in the vertical banding in Figure 4.21, particularly at beryllium thicknesses of 0, $\sim$0.0025, and $\sim$0.013 cm. If the code were somehow able to link the thickness and material, the optimization may be more efficient. Also, a more cohesive package would greatly increase usability. A singular Python package, could be developed to combine initial settings and subsequent results visualization.

Appendix A. Optimization Code Examples

This appendix consists of example code for the optimization runs. It follows the flow chart in Figure 3.4.

The example is from the 2 MeV deuterons run. It has a run identification number of 4614. The process is described in Section 3.3.

Listing A.1. newrun4614.sh

```
#!/bin/sh

num='4614'
newdir="daksrun${num}"

nps='1e7'
energy='2'
particle='d' # use h for protons, and d for deuterons

# Create a new directory for this particular run
mkdir daksrun${num}

#copy common files to new run
cp -r templatedir daksrun${num}/templatedir
cp l2sim_driver.sh daksrun${num}/l2sim_driver.sh
cp daksl.in daksrun${num}/daksl${num}.in
cp daksub.pbs daksrun${num}/daksub${num}.pbs
chmod 755 ${newdir}/daksub${num}.pbs
chmod 755 ${newdir}/templatedir/runMCNP.pbs
chmod 755 ${newdir}/l2sim_driver.sh

# cd to the new directory
cd daksrun${num}

# Update the run numbers in the template files
sed -i "s/numero/${num}/g" daksub${num}.pbs  # update the dakota
    submission pbs file
sed -i "s/numero/${num}/g" templatedir/runMCNP.pbs # Add the run
    number to MCNP submission

```

```
29 # Update settings in ParamsInReplace.sh
30 sed -i "s/3nergy/${energy}/g" templatedir/ParamsInReplace2.sh # Add
      the energy for this run
31 sed -i "s/partic1e/${particle}/g" templatedir/ParamsInReplace2.sh #
      Add the energy for this run
32 sed -i "s/NumPartS/${nps}/g" templatedir/ParamsInReplace2.sh # Add
      the nps for this run
33
34
35 # Submit the Dakota PBS job!
36 qsub daksub${num}.pbs
37
38 echo "*******From newrun${num}: daksub${num}.pbs Submitted*******"
```

Listing A.2. daksub4614.pbs

```
#!/bin/bash

#PBS -N DakLay4614
#PBS -l walltime=29:00:00
#PBS -l select=1:ncpus=48:mpiprocs=48
#PBS -q standard
#PBS -A <project number>
#PBS -j oe
#PBS -r n
#PBS -V

date
# Note when the run started

cd $PBS_O_WORKDIR

export DAKOTA_NPROCS=48 #MAKE THIS EQUAL TO NUMBER OF PROCESSORS
   REQUESTED
# export NProcs=$DAKOTA_NPROCS
export MPI_SHEPHERD=true
export MPI_DSM_DISTRIBUTE=true

dakota -i daksl4614.in -o daksl4614.out

date
# Note when the run ended
```

Listing A.3. daksl4614.in

```
# Dakota Input File: MCNP Multi-Layer Thickness Study Test
# Initial template by Thomas Schlitt -- for Zack Bretz, edited by
   Zack Bretz
# November 2021
# Usage: dakota -i daksl000.in -o daksl000.out
# Building in conjunction with Zack Bretz optimization problem
# This deck should optimize a three layer target of various
   materials, bombarded by protons or deuterons


environment
    tabular_data
    tabular_data_file = 'soga3Layers.dat'

method
    soga
        population_size = 50
        convergence_type best_fitness_tracker
    percent_change = .01  num_generations = 15
        print_each_pop
# convergence_type  average_fitness_tracker
#   num_generations = 20
#   percent_change = .1

#       defaults
# fitness_type merit_function
# replacement_type elitist
# initialization_type  unique_random
# crossover_type  shuffle_random
#   num_parents = 2
```

```
#   num_offspring = 2
#   crossover_rate = 0.8
# mutation_type  replace_uniform
#   mutation_rate = 0.08
# convergence_tolerance = 1.e-4



model
    single #<<-- single analysis rather than multiple (DACE, etc)



variables
#    continuous_design = 2  # This is how you specify the variable type to work with
#         descriptors     'thick1'     'thick2'
#         lower_bounds     0.001         0.001
#         upper_bounds      .5           .5

    discrete_design_range = 3
  # this range will determine the percentage of the thickness to be used for each
  # layer, of which we will limit to 3
  descriptors         'thick1'    'thick2'   'thick3'
  lower_bounds           1           1          1
        upper_bounds          100         100        100

    discrete_design_set
# integer 1
# descriptors           'mat1'    'mat2'
# elements_per_variable  3          3
```

```
# elements                32 42 62      32 42 62

  string 3
  descriptors          'mat1'     'mat2'           'mat3'
  elements_per_variable 4          4                4
        elements      '32Sp@ces-0.535' '42Sp@ces-1.848' '6222Sp@ces
   -1.05' '62Sp@ces-2.0'
                      '32Sp@ces-0.535' '42Sp@ces-1.848' '6222Sp@ces
   -1.05' '62Sp@ces-2.0'
                      '32Sp@ces-0.535' '42Sp@ces-1.848' '6222Sp@ces
   -1.05' '62Sp@ces-2.0'

interface
    fork
  asynchronous evaluation_concurrency = 4

  analysis_drivers = 'l2sim_driver.sh'
        parameters_file = 'params.in'
        results_file = 'results.out'
      file_tag file_save
  work_directory named 'workdir'
      directory_tag  directory_save
      link_files = 'templatedir/*'
            deactivate active_set_vector

responses
    objective_functions = 1
    sense = "max"
    descriptors = 'TotNFlux'
    no_gradients
    no_hessians
```

Listing A.4. l2sim_driver.sh

```
#!/bin/sh
# Sample simulator to Dakota system call script
# The first and second command line arguments to the script are the
# names of the Dakota parameters and results files.
#
#
#
# DO NOT TOUCH!
params=$1       #These are the connection points that DAKOTA will
    interface with !
results=$2
# echo

# echo "===== results = ${results} ====="

numarr=(${results//./ })
evalnum=${numarr[2]}
# echo "1sim - eval number: ${evalnum}"

# --------------
# PRE-PROCESSING
# --------------
# Incorporate the parameters from Dakota into the template, writing
    ros.in
# dprepro $params dob.template <<Target>>
dprepro --inline "?? ??" $params ParamsInReplace2.sh
    ParamsInReplaced${evalnum}.sh

# echo "1.5sim ls of $(pwd): $(ls) ---- end ls ---- Should have
    ParamsInReplaced${evalnum}.sh"
```

```
27
28 #above line is done in each workdir.N, where N is the evalnum
29 # ParamsInReplace.sh is in the templatedir folder
30 # echo "2sim ========= PIR${evalnum}.sh has been created and
       dpreproed ======"
31
32 # Copy the evaluation number N into the params folder
33 sed -i "s/evaluati0nnumber/$evalnum/g" ParamsInReplaced${evalnum}.sh
34 # echo "3sim========= The eval num has been sed'd to PIR${evalnum}.
       sh ======"
35
36 #echo '4sim##########################################'
37 # echo "5sim pwd: $(pwd) <should match> ${evalnum}"  # Ascertain the
        workdir
38 #echo "6sim ls of $(pwd): $(ls)"
39
40
41 # ---------
42 # EXECUTION
43 # ---------
44
45 # Fill in MCNP template by running ParamsInReplace${evalnum}.sh (
       Parameters input replace in MCNP)
46 chmod 755 ParamsInReplaced${evalnum}.sh  # Make sure it can be run
47 ./ParamsInReplaced${evalnum}.sh  # run it
48
49 # echo "7sim====== ${evalnum} MCNPtargets3.i created ======"
50
51
52 # Run MCNP!
53 # mpiexec -np 48 mcnp6.mpi xsdir=xsdir_mcnp6.2_JDEU_CP2020 i=
       MCNPtargets3.i  o="${evalnum}_MCNP.o"
```

```
# mcnp6 xsdir=xsdir_mcnp6.2_JDEU_CP2020 i=MCNPtargets3.i  o="${evalnum}_MCNP.o" tasks 4
# mpirun -np 4 singularity run /p/work1/projects/afitenp/MCNP/MCNP620/mcnp620mustang_mpi.sif ixr xsdir=xsdir_mcnp6.2_Bretz i=MCNPtargets3.i  o="${evalnum}_MCNP.o"
# srun -n 12 mcnp6 xsdir=xsdir_mcnp6.2_Bretz i=MCNPtargets3.i  o="${evalnum}_MCNP.o"

sed -i "s/NUMEVAL/${evalnum}/g" runMCNP.pbs   # Update with the current eval number, same as N in workdir.N
#chmod 755 runMCNP.pbs  #not sure this is necessary but it's here
qsub runMCNP.pbs  # Submit the MCNP job to the debug queue
echo "*******qsubbed runMCNP.pbs in eval ${evalNum}*******"

ticker=0
while [[ ! -e ${evalnum}_MCNP.o ]]; do
    if [[ $ticker -ge 45 ]]; then
        echo "Took more than 1.5m for ${evalnum}_MCNP.o to write"
        touch ${evalnum}_MCNP.o
        echo "Touched ${evalnum}_MCNP.o, will write filler in next step."
    fi
    ((ticker++))
    sleep 2
done
echo "Took ${ticker} seconds for ${evalnum}_MCNP.o to write"
sleep 10 # We need to make sure ${evalnum}_MCNP.o is finished
MCNPfin=false
while [[ ! $(tail -n 1 ${evalnum}_MCNP.o | grep ' mcnp     ') ]]; do
    if [[ i -ge 48 ]]; then
        echo "********************${evalnum}_MCNP.o failed to finish after 8 minutes**********************"
```

```
79          echo "${evalnum}_MCNP.o failed to write" >> ${evalnum}_MCNP.
    o
80          echo " surface  99.2" >> ${evalnum}_MCNP.o
81          echo "      total        9.99999E+00 0.0000"  >> ${evalnum}
    _MCNP.o
82          echo " mcnp     v" >> ${evalnum}_MCNP.o
83          echo "***** **** *** ** * Wrote error and filler out code
    for ${evalnum}_MCNP.o* ** *** **** *****"
84          # break
85     fi
86     ((i++))
87     if [[ i -ge 50 ]]; then
88          echo "**********************${evalnum}_MCNP.o failed to
    finish after 8.33 minutes, something else wrong
    **********************"
89          break
90     fi
91     sleep 10
92 done
93
94 echo " ===== ${evalnum}_MCNP should have finished writing ===== "
95
96 rm runtp*  # these take a lot of storage, unneeded
97 # echo "8sim=======created ${evalnum}_MCNP.o======="
98 # echo "9sim=======SHOULD'VE RUN MCNP INP ${evalnum}======="
99
100
101
102 # ---------------
103 # POST-PROCESSING
104 # ---------------
105 # extract function value from the simulation output
```

```
106 # the MCNP output file must be in the format N_MCNP.o, where N is
      the workdir.N number
107 python get_flux.py
108 # echo "10sim=======SHOULD'VE RUN GET_FLUX ${evalnum}======="
109 # echo;echo;echo
110 # echo '11sim === end sim ==='
111 # echo;echo;echo
```

Listing A.5. ParamsInReplace2.sh

```
# This file should be initially placed in the templatedir directory.
# The values which will be subbed into the MCNP template will be
# edited by dprepro.

# The variable following evalNum should be sed'ed in by lsim_driver.
    sh,
# and this file renamed ParamsInReplaced${evalNum}.sh
evalNum=evaluati0nnumber

#echo "Params Check 1"

# Does evanNum==the N in workdir.N?
cwdp=$(pwd)  # Current working directory path
cwdparr=(${cwdp//// })
cwd=${cwdparr[${#cwdparr[@]}-1]}  # last element in the path
cwdarr=(${cwd//./ })
evalwN=${cwdarr[1]}

# echo 'next line is line 19'
if [[ $evalNum -eq $evalwN ]]
then
    echo "par2 ====== We are in the right place! ${cwd} ======"
fi


# ----------------------------
# Other Settings (Defined & sed'd in newrun###.sh)
# ----------------------------
nps='1e7'     # number of particles to run
energy='2'    # Energy in MeV
```

```
particle='d'  # Particle is either p or d
#echo "***Should have ${nps} nps, ${energy} MeV energy, and ${particle} particles in eval ${evalNum}***"

# ----------------------------
# dprepro variables
# ----------------------------
# These thickness percentages should be integers 1-100, corresponding
# to the percentage of the max thickness
#echo 'par3 dprepro vars next'
thickp1='??thick1??'
thickp2='??thick2??'
thickp3='??thick3??'

# Materials
matl1='??mat1??'
matl2='??mat2??'
matl3='??mat3??'


# Function to get the layer's max thickness for a particular material
get_tmax() {
    matl=$1

   if [[ $particle == 'h' ]]; then
        if [[ $energy -le 2 ]]; then
            if [[ $matl == '32Sp@ces-0.535' ]]; then tmax=".017"  # SRIM: 159.08 um
            elif [[ $matl == '42Sp@ces-1.848' ]]; then tmax="0.005"  #SRIM: 48.52 um
```

```
57            elif [[ $matl == '6222Sp@ces-1.05' ]]; then tmax=".01"  #SRIM: NA
58            elif [[ $matl == '62Sp@ces-2.0' ]]; then tmax="0.004"  #SRIM: 37.62 um
59            fi
60    elif [[ $energy -gt 2 ]]; then
61            if [[ $matl == '32Sp@ces-0.535' ]]; then tmax=".083"  #SRIM: 785.20 um
62            elif [[ $matl == '42Sp@ces-1.848' ]]; then tmax="0.025"  #SRIM: 233.61 um
63            elif [[ $matl == '6222Sp@ces-1.05' ]]; then tmax=".01"  #SRIM: NA
64            elif [[ $matl == '62Sp@ces-2.0' ]]; then tmax="0.019"  #SRIM: 178.97 um
65            fi
66    fi
67
68     elif [[ $particle == 'd' ]]; then
69         if [[ $energy -le 2 ]]; then
70            if [[ $matl == '32Sp@ces-0.535' ]]; then tmax="0.011"  #SRIM: 102.54 um
71            elif [[ $matl == '42Sp@ces-1.848' ]]; then tmax=".004"  #SRIM: 32.07 um
72            elif [[ $matl == '6222Sp@ces-1.05' ]]; then tmax=".005"  #SRIM: 47.08 um
73            elif [[ $matl == '62Sp@ces-2.0' ]]; then tmax="0.003"  #SRIM: 24.78 um
74            fi
75    elif [[ $energy -gt 2 ]]; then
76            if [[ $matl == '32Sp@ces-0.535' ]]; then tmax="0.05"  #SRIM: 466.81 um
77            elif [[ $matl == '42Sp@ces-1.848' ]]; then tmax="0.015"
```

```
    #SRIM: 141.37 um
78              elif [[ $matl == '6222Sp@ces-1.05' ]]; then tmax=".022"
    #SRIM: 210.01 um
79              elif [[ $matl == '62Sp@ces-2.0' ]]; then tmax="0.012"  #
   SRIM: 109.41 um
80              fi
81          fi
82
83      else
84          echo "Incorrect particle designation in ParamsInReplace.sh."
85          echo tmax="NaN"
86      fi
87
88      echo $tmax
89  }
90
91  # Define the maximum thicknesses for each layer
92  tmax1="$(get_tmax $matl1)"
93  tmax2="$(get_tmax $matl2)"
94  tmax3="$(get_tmax $matl3)"
95  echo "Max thicknesses for eval $evalNum are ${tmax1} ${tmax2} ${
    tmax3}"
96
97  # ----------------------------
98  # Do calculations
99  # ----------------------------
100 #echo 'par4 calcs next'
101 thick1=$(echo "scale=5;$tmax1*$thickp1/100;" | bc)
102 thick2=$(echo "scale=5;$tmax2*$thickp2/100;" | bc)
103 thick3=$(echo "scale=5;$tmax3*$thickp3/100;" | bc)
104
105 vx_3=$(echo "$thick1+$thick2" | bc)
```

```
106
107
108
109 # ----------------------------
110 # Perform substitutions
111 # ----------------------------
112 # Save a new copy of mcnp template
113 # This file should be copied into the workdir.N folder, so we need
      to
114 # copy the MCNP template from templatedir into this workdir.N
115 # mcnptemplatein='mcnp.template.3layers.in'
116 #echo 'par5 perform sed subs'
117 Mt3='MCNPtargets3.i'
118 cp ../templatedir/mcnp.template.3layers.in $Mt3
119
120
121
122 # Sub thicknesses
123 sed -i  "s/thick1/$thick1/g" $Mt3
124 sed -i  "s/thick2/$thick2/g" $Mt3
125 sed -i  "s/thick3/$thick3/g" $Mt3
126
127
128 # Sub materials
129 sed -i "s/mat1/$matl1/g" $Mt3
130 sed -i "s/mat2/$matl2/g" $Mt3
131 sed -i "s/mat3/$matl3/g" $Mt3
132 sed -i 's/Sp@ces/  /g'  $Mt3 # Remove those spaceholders
133
134
135 # Sub surface vector values
136 sed -i "s/vx_3/$vx_3/g" $Mt3
```

```
137
138
139 # Other settings subs
140 sed -i "s/numPart/$nps/g" $Mt3
141 sed -i "s/3n3rgy/$energy/g" $Mt3
142 sed -i "s/p@rticle/$particle/g" $Mt3
143
144 echo 'end params sh'
```

Listing A.6. mcnp.template.3layers.i

```
Bretz thesis, 2 layer test deck template for Dakota optimization
c
c -
c
c ******************************************
c Cell Cards
c ******************************************
c
  1  mat1  -1     imp:n=1    $ First target layer cell
c Note: mat1 will be a string which includes the material number and
     the density
c       Example: "42   -1.484"
c
  2  mat2  -2     imp:n=1    $ Second target layer cell
c
  3  mat3  -3     imp:n=1    $ Third target layer cell
c
  9  0        1 2 3 -99  imp:n=1  $ Vacuum environment
c
  99 0          99    imp:n=0    $ Kill zone

c ******************************************
c Surfaces
c ******************************************
c
c n RCC      vx   vy vz    hx    hy hz  R
  1 RCC      0    0  0   thick1  0  0   5   $ First Target layer
c
  2 RCC   thick1  0  0   thick2  0  0   5   $ Second target layer
c
```

```
  3 RCC     vx_3  0  0   thick3  0  0   5
c
c
  99 RCC   -6 0 0  26 0 0  11.547    $ Boundary cylinder
c

c ******************************************
c Data Cards
c ******************************************
c --------------------
c Material Cards
c --------------------
c
c Need to figure out the multiple materials and xsec libraries, as
    well as the
c multiple
c
c Lithium, density = 0.535
  m31 3007.00h  1     $ Li p CP2020
  m32 3007.83o  1     $ Li d JENDL
c
c Beryllium, density = 1.848000
  m41 4009.00c   1     $ Be p ENDF8
  m42 4009.83o   1     $ Be d JENDL
c
c Carbon, density = 2
  m62 6012.83o  1    $ C d JENDL
c
c CD2, deuterated polyethylene, density = ?????
  m6222 6012.83o  1    $ The carbon part, JENDLDEU
        1002.00o  2    $ The deuterons part, CP2020
c
```

```
c
c HLIB card to add proton library
c
c
c --------------------
c Physics Cards
c --------------------
c minimum: mode and how long to run
  mode n p@rticle  $h d $t
  nps numPart  $ do we want to vary this?
c  cut:d j .1  $ this line needed since MCNP by default cuts
   deuterons below 2 MeV
  cut:p@rticle j .001
c
c
c --------------------
c Source
c --------------------
c --- Disk source perpendicular to z-axis uniformly emitting
c     ERG-MeV deuterons mono-directionally in the +ve x-direction
c
  SDEF  POS = -5 0 0  AXS=1 0 0  RAD=d1  PAR=p@rticle  ERG=3n3rgy
   VEC=1 0 0  DIR=1
  SI1  0 0.1     $ radial sampling distance, second number is Rmax
   in cm
  SP1 -21 1      $ radial sampling weighting: r^1 for disk
c
c --------------------
c Tallies
c --------------------
  f11:n  99.1 99.2 99.3 $ All neutrons that incident the outer
   cylinder
```

```
  e11     .5 34i 18  $energy bins
  fm11    1.48287e7    $ per uC charge, ie, per deuteron? w/ 10e9 as
   in lit plots
c The "detector" using this setup would be face 99.2
c
PRINT   $ print it all
c PRINT 110
```

Listing A.7. runMCNP.pbs

```
#!/bin/bash

#PBS -N MCNP4614_NUMEVAL
#PBS -l select=1:ncpus=48
#PBS -l walltime=00:20:00
#PBS -q debug
#PBS -A <project number>
#PBS -r n
#PBS -V
#PBS -j oe

echo '**********'
echo 'Run start:'
date
echo '**********'

mpiexec -np 48 singularity run /p/work1/projects/afitenp/MCNP/
    MCNP620/mcnp620mustang_mpi.sif ixr xsdir=xsdir_mcnp6.2_Bretz i=
    MCNPtargets3.i o=NUMEVAL_MCNP.o

echo '**********'
echo 'Run end:'
date
echo '**********'
```

Listing A.8. get_flux.py

```
#!/usr/bin/env python
############################
# PYTHON EXECUTION DRIVER:
############################
'''
Author:    Thomas Schlitt
Date:      11/7/21

Edited by Zack Bretz Jan 2022

Purpose:
--------------------
This script analyzes Be target output -- looks for "surface  99.2" (
    yes, with two spaces in there) then finds the total neutron
    production afterwards
'''
########################################
# IMPORTS
########################################
import os
import sys

fdir = os.getcwd()   #There's your home-directory for you

# fdir = current working directory (workdir.1,workdir.4,etc)
# num takes the full path of the workdir path and returns the
    integer tail
num = fdir.split('.')[-1]
# ex. ~/research/dakota/workdir.10
# num .: = 10
```

```
28
29 tally_bool = False   #Stay false until we find the "Surface 99.2"
    flag
30 ############################################################
31 #               TIME TO PROCESS OUTCOME OF SIMULATIONS
32 ############################################################
33 with open(os.path.join(fdir,"{0}_MCNP.o".format(num))) as f:
34   lines = f.readlines()
35   for l in lines:
36     if 'surface  99.2' in l:
37       tally_bool = True #turn on the tally bool
38     if 'total' in l and tally_bool == True:
39       res = float(l.split()[1])  # save the negative of the total
    flux number
40       print res
41       break #once we've found the result, break the loop and move on
42
43
44 fpath = fdir + r"/results.out.{0}".format(num)
45 # fpath creates the target file path & name for the results.out.#
    that DAKOTA is looking for
46
47 with open(fpath,'w') as f:            #with open() creates a text
    editor instance under object "f"
48     f.write('{0:.8f}'.format(res))  #write to the text file "f" one
    number
49                                      # "0" means its the first
    argument in the .format() call
50                                      # ":.8f" means write 16 decimal
     places
```

Bibliography

1. K. T. Bainbridge, "Trinity," Los Alamos Scientific Lab., NM (USA), Tech. Rep., 1976.

2. S. Singh and C. R. Way, "The correlates of nuclear proliferation: A quantitative test," *Journal of Conflict Resolution*, vol. 48, no. 6, pp. 859–885, 2004.

3. Joint Defense Science Board/Threat Reduction Advisory Committee Task Force, "The Nuclear Weapons Effects National Enterprise," Office of the Under Secretary of Defense for Acquisition, Technology, and Logistics, Tech. Rep. June, 2010.

4. S. Glasstone, P. J. Dolan *et al.*, *The effects of nuclear weapons*. US Department of Defense, 1977, vol. 50, no. 3.

5. J. Walker, "Uses of neutrons in engineering and technology," *Physics in Technology*, vol. 13, no. 6, pp. 239–248, nov 1982. [Online]. Available: https://doi.org/10.1088/0305-4624/13/6/i01

6. M. Johnson, "The industrial uses of neutrons," *Applied Radiation and Isotopes*, vol. 46, no. 6, pp. 673–680, 1995. [Online]. Available: https://www.sciencedirect.com/science/article/pii/0969804395001328

7. J. Trewhella, "Neutrons reveal how nature uses structural themes and variation in biological regulation," *Physica B: Condensed Matter*, vol. 385-386, pp. 825–830, 2006. [Online]. Available: https://www.sciencedirect.com/science/article/pii/S0921452606009367

8. D. Sarenac, C. W. Clark, D. G. Cory, C. Kapahi, B. Heacock, M. G. Huber, J. Nsofini, C. B. Shahi, and D. A. Pushin, "Structured neutron waves," in *Optical, Opto-Atomic, and Entanglement-Enhanced Precision Metrology*, vol. 10934. SPIE, 2019, pp. 232–240.

9. J. Morrell, *Next-Generation Isotope Production via Deuteron Breakup*. University of California, Berkeley, 2021.

10. R. S. Stone and J. C. Larkin Jr, "The treatment of cancer with fast neutrons," *Radiology*, vol. 39, no. 5, pp. 608–620, 1942.

11. W. Howard, S. Grimes, T. Massey, S. Al-Quraishi, D. Jacobs, C. Brient, and J. Yanch, "Measurement of the thick-target 9Be (p, n) neutron energy spectra," *Nuclear science and engineering*, vol. 138, no. 2, pp. 145–160, 2001.

12. T. Kageji, S. Nagahiro, Y. Mizobuchi, K. Matsuzaki, Y. Nakagawa, and H. Kumada, "Boron neutron capture therapy (BNCT) for newly-diagnosed glioblastoma: comparison of clinical results obtained with BNCT and conventional treatment," *The Journal of Medical Investigation*, vol. 61, no. 3.4, pp. 254–263, 2014.

13. B. W. Blackburn, J. C. Yanch, and R. E. Klinkowstein, "Development of a high-power water cooled beryllium target for use in accelerator-based boron neutron capture therapy," *Medical Physics*, vol. 25, no. 10, pp. 1967–1974, 1998.

14. L. Zaidi, M. Belgaid, S. Taskaev, and R. Khelifi, "Beam shaping assembly design of 7Li (p, n) 7Be neutron source for boron neutron capture therapy of deep-seated tumor," *Applied Radiation and Isotopes*, vol. 139, pp. 316–324, 2018.

15. R. Commisso, R. Allen, J. Boller, G. Cooperstein, R. Fisher, D. Hinshelwoor, T. Holt, D. Murphy, J. Neri, P. Ottinger *et al.*, "Status of the Mercury pulsed-power generator, a 6-MV 360-kA, magnetically-insulated inductive voltage adder," in *Digest of Technical Papers. PPC-2003. 14th IEEE International Pulsed Power Conference (IEEE Cat. No. 03CH37472)*, vol. 1. IEEE, 2003, pp. 383–386.

16. J. Boller, J. Burton, and J. Shipman Jr, "Status of the upgraded version of the NRL Gamble II Pulse Power Generator," NAVAL RESEARCH LAB WASHINGTON DC, Tech. Rep., 2013.

17. J. M. Carpenter and W. B. Yelon, "2. Neutron Sources," in *Methods in Experimental Physics*. Elsevier, 1986, vol. 23, pp. 99–196.

18. J. Chadwick, "Possible existence of a neutron," *Nature*, vol. 129, no. 3252, pp. 312–312, 1932.

19. I. QSA Global, "AMBE INDUSTRIAL NEUTRON SOURCES," Available at https://www.qsa-global.com/industrial-ambe-neutron-sources (2022/02/02).

20. K. S. Krane, *Introductory nuclear physics*. John Wiley & Sons, 1991.

21. A. Zylstra, O. Hurricane, D. Callahan, A. Kritcher, J. Ralph, H. Robey, J. Ross, C. Young, K. Baker, D. Casey *et al.*, "Burning plasma achieved in inertial fusion," *Nature*, vol. 601, no. 7894, pp. 542–548, 2022.

22. R. Cheverton and T. Sims, "HFIR CORE NUCLEAR DESIGN." Oak Ridge National Lab., Tenn., Tech. Rep., 1971.

23. M. K. Covo, R. A. Albright, B. F. Ninemire, M. B. Johnson, A. Hodgkinson, T. Loew, J. Y. Benitez, D. S. Todd, D. Z. Xie, T. Perry *et al.*, "88-Inch Cyclotron: The one-stop facility for electronics radiation testing," in *2017 IEEE International Workshop on Metrology for AeroSpace (MetroAeroSpace)*. IEEE, 2017, pp. 484–488.

24. K. Harrig, B. Goldblum, J. Brown, D. Bleuel, L. Bernstein, J. Bevins, M. Harasty, T. Laplace, and E. Matthews, "Neutron spectroscopy for pulsed beams with frame overlap using a double time-of-flight technique," *Nuclear Instruments and Methods in Physics Research Section A: Accelerators, Spectrometers, Detectors and Associated Equipment*, vol. 877, pp. 359–366, 2018.

25. C. Lavelle, D. V. Baxter, A. Bogdanov, V. Derenchuk, H. Kaiser, M. Leuschner, M. Lone, W. Lozowski, H. Nann, B. Przewoski *et al.*, "Neutronic design and measured performance of the Low Energy Neutron Source (LENS) target moderator reflector assembly," *Nuclear Instruments and Methods in Physics Research Section A: Accelerators, Spectrometers, Detectors and Associated Equipment*, vol. 587, no. 2-3, pp. 324–341, 2008.

26. T. Mason, D. Abernathy, I. Anderson, J. Ankner, T. Egami, G. Ehlers, A. Ekkebus, G. Granroth, M. Hagen, K. Herwig *et al.*, "The Spallation Neutron Source in Oak Ridge: A powerful tool for materials research," *Physica B: Condensed Matter*, vol. 385, pp. 955–960, 2006.

27. J. J. Ramirez, A. J. Toepfer, and M. J. Clauser, "Pulsed power applications to intense neutron source development," *Nuclear Instruments and Methods*, vol. 145, no. 1, pp. 179–183, 1977.

28. D. Pelowitz, "MCNP6 User's Manual," *Los Alamos National Security LLC*, 2008.

29. B. Adams, W. Bohnhoff, K. Dalbey, M. Ebeida, J. Eddy, M. Eldred, R. Hooper, P. Hough, K. Hu, J. Jakeman *et al.*, "Dakota, A Multilevel Parallel Object-Oriented Framework for Design Optimization, Parameter Estimation, Uncertainty Quantification, and Sensitivity Analysis: Version 6.13 User's Manual." Sandia National Lab.(SNL-NM), Albuquerque, NM (United States), Tech. Rep., 2020.

30. K. Weaver, J. Anderson, H. Barschall, and J. Davis, "Neutron spectra from deuteron bombardment of D, Li, Be, and C," *Nuclear Science and Engineering*, vol. 52, no. 1, pp. 35–45, 1973.

31. Y. Tajiri, Y. Watanabe, N. Shigyo, K. Hirabayashi, T. Nishizawa, and K. Sagara, "Measurement of double differential neutron yields from thick carbon target irradiated by 5-MeV and 9-MeV deuterons," *Progress in Nuclear Science and Technology*, vol. 4, pp. 582–586, 2014.

32. P. R. Page, "New broad ^{8}Be nuclear resonances," *Phys. Rev. C*, vol. 72, p. 054312, Nov 2005. [Online]. Available: https://link.aps.org/doi/10.1103/PhysRevC.72.054312

33. C. A. Bertulani, "Nuclear reactions," *arXiv preprint arXiv:0908.3275*, 2009.

34. S. I. Lipschutz, *The (p, n) charge-exchange reaction in inverse kinematics as a probe for isovector giant resonances in exotic nuclei*. Michigan State University, 2018.

35. R. Serber, "The production of high energy neutrons by stripping," *Physical Review*, vol. 72, no. 11, p. 1008, 1947.

36. J. R. Oppenheimer, "The disintegration of the deuteron by impact," *Physical Review*, vol. 47, no. 11, p. 845, 1935.

37. S. Dancoff, "Disintegration of the Deuteron in Flight," *Physical Review*, vol. 72, no. 11, p. 1017, 1947.

38. R. Gold and C. Wong, "Disintegration of the Deuteron in a Coulomb Field," *Physical Review*, vol. 132, no. 6, p. 2586, 1963.

39. M. McMahan, L. Ahle, D. Bleuel, L. Bernstein, B. Barquest, J. Cerny, L. Heilbronn, C. Jewett, I. Thompson, and B. Wilson, "Neutron beams from deuteron breakup at the 88-Inch cyclotron at Lawrence Berkeley National Laboratory," in *International Conference on Nuclear Data for Science and Technology*. EDP Sciences, 2007, pp. 411–414.

40. N. Metropolis and S. Ulam, "The monte carlo method," *Journal of the American statistical association*, vol. 44, no. 247, pp. 335–341, 1949.

41. R. Y. Rubinstein and D. P. Kroese, *Simulation and the Monte Carlo method*. John Wiley & Sons, 2016.

42. D. A. Brown, M. Chadwick, R. Capote, A. Kahler, A. Trkov, M. Herman, A. Sonzogni, Y. Danon, A. Carlson, M. Dunn *et al.*, "ENDF/B-VIII. 0: The 8th major release of the nuclear reaction data library with CIELO-project cross sections, new standards and thermal scattering data," *Nuclear Data Sheets*, vol. 148, pp. 1–142, 2018.

43. D. K. Parsons and C. A. Toccoli, "Verification of the CP2020 Library," Los Alamos National Lab.(LANL), Los Alamos, NM (United States), Tech. Rep., 2021.

44. A. Koning, D. Rochman, J.-C. Sublet, N. Dzysiuk, M. Fleming, and S. Van der Marck, "TENDL: complete nuclear data library for innovative nuclear science and technology," *Nuclear Data Sheets*, vol. 155, pp. 1–55, 2019.

45. S. Nakayama, O. Iwamoto, Y. Watanabe, and K. Ogata, "JENDL/DEU-2020: Deuteron nuclear data library for design studies of accelerator-based neutron sources," *Journal of Nuclear Science and Technology*, vol. 58, no. 7, pp. 805–821, 2021.

46. X.-. M. C. Team, "MCNP—A General Monte Carlo N-Particle Transport Code, Version 5," 2003.

47. T. Goorley, M. James, T. Booth, F. Brown, J. Bull, L. Cox, J. Durkee, J. Elson, M. Fensin, R. Forster *et al.*, "Initial MCNP6 release overview," *Nuclear technology*, vol. 180, no. 3, pp. 298–315, 2012.

48. J. E. Bevins, *Targeted modification of neutron energy spectra for national security applications*. University of California, Berkeley, 2017.

49. K. Harrig, B. Goldblum, J. Brown, D. Bleuel, L. Bernstein, J. Bevins, M. Harasty, T. Laplace, and E. Matthews, "Neutron spectroscopy for pulsed beams with frame overlap using a double time-of-flight technique," *Nuclear Instruments and Methods in Physics Research Section A: Accelerators, Spectrometers, Detectors and Associated Equipment*, vol. 877, pp. 359–366, 2018.

50. J.-P. Meulders, P. Leleux, P. Macq, and C. Pirart, "Fast neutron yields and spectra from targets of varying atomic number bombarded with deuterons from 16 to 50 MeV (for radiobiology and radiotherapy)," *Physics in Medicine & Biology*, vol. 20, no. 2, p. 235, 1975.

51. M. a. Baba, Y. Nauchi, T. Iwasaki, T. Kiyosumi, M. Yoshioka, S. Matsuyama, N. Hirakawa, T. Nakamura, S. Tanaka, S. Meigo *et al.*, "Characterization of a 40–90 MeV 7Li (p, n) neutron source at TIARA using a proton recoil telescope and a TOF method," *Nuclear Instruments and Methods in Physics Research Section A: Accelerators, Spectrometers, Detectors and Associated Equipment*, vol. 428, no. 2-3, pp. 454–465, 1999.

52. C. Lederer, F. Käppeler, M. Mosconi, R. Nolte, M. Heil, R. Reifarth, S. Schmidt, I. Dillmann, U. Giesen, A. Mengoni *et al.*, "Definition of a standard neutron field with the 7 Li (p, n) 7 Be reaction," *Physical Review C*, vol. 85, no. 5, p. 055809, 2012.

53. H. Lefevre and G. Din, "Zero Degree Neutron Yield from the 7Li (p, n) 7Be Reaction Near 2· 2 MeV," *Australian Journal of Physics*, vol. 22, no. 6, pp. 669–678, 1969.

54. D. J. Gillich, A. Kovanen, and Y. Danon, "Deuterated target comparison for pyroelectric crystal D–D nuclear fusion experiments," *Journal of nuclear materials*, vol. 405, no. 2, pp. 181–185, 2010.

55. D. Jones and C. Bartle, "Neutrons from the 2 MeV deuteron bombardment of thick 7Li targets," *Nuclear Instruments and Methods*, vol. 118, no. 2, pp. 525–529, 1974.

56. J. W. Meadows, "The 9Be (d, n) thick-target neutron spectra for deuteron energies between 2.6 and 7.0 MeV," *Nuclear Instruments and Methods in Physics Research Section A: Accelerators, Spectrometers, Detectors and Associated Equipment*, vol. 324, no. 1-2, pp. 239–246, 1993.

57. R. G. Cooper and A. P. Harrison, "The uses and adverse effects of beryllium on health," *Indian journal of occupational and environmental medicine*, vol. 13, no. 2, p. 65, 2009.

58. K. Harris, H. Grench, R. Johnson, and F. Vaughn, "The V51 (p, n) Cr51 reaction as a neutron source of known intensity," *Nuclear Instruments and Methods*, vol. 33, no. 2, pp. 257–260, 1965.

59. G. Deconninck and J. Royen, "THE REACTION *sup*51 V(p,n) *sup*51 Cr AS A SOURCE OF MONOENERGETIC NEUTRONS." Univ., Louvain, Belgium. Facultes Univ., Namur, Belgium, Tech. Rep., 1969.

60. V. Lelasseux, P.-A. Söderström, S. Aogaki, K. Burdonov, M. Cerchez, S. Chen, S. Dorard, A. Fazzini, M. Gugiu, S. Pikuz *et al.*, "Design and commissioning of a neutron counter adapted to high-intensity laser matter interactions," *Review of Scientific Instruments*, vol. 92, no. 11, p. 113303, 2021.

61. S. Araki, Y. Watanabe, T. Kin, N. Shigyo, and K. Sagara, "Measurement of double differential neutron yields from thick aluminum target irradiated by 9 MeV deuteron," *Energy Procedia*, vol. 71, pp. 197–204, 2015.

62. M. Saltmarsh, C. Ludemann, C. Fulmer, and R. Styles, "Characteristics of an intense neutron source based on the d+ Be reaction," *Nuclear Instruments and Methods*, vol. 145, no. 1, pp. 81–90, 1977.

63. Los Alamos National Laboratory, "MCNP6.1.4," https://mcnp.lanl.gov/, 2008.

64. Air Force Research Laboratory, "HPE SGI 8600 (Mustang) User Guide," https://www.afrl.hpc.mil/docs/mustangUserGuide.html#scope, 2021.

65. J. F. Ziegler, M. D. Ziegler, and J. P. Biersack, "SRIM–The stopping and range of ions in matter (2010)," *Nuclear Instruments and Methods in Physics Research Section B: Beam Interactions with Materials and Atoms*, vol. 268, no. 11-12, pp. 1818–1823, 2010.

66. B. Adams, W. Bohnhoff, K. Dalbey, M. Ebeida, J. Eddy, M. Eldred, R. Hooper, P. Hough, K. Hu, J. Jakeman, M. Khalil, K. Maupin, J. A. Monschke, E. Ridgway, A. Rushdi, D. Seidl, J. Stephens, and J. Winokur, "Dakota, A Multilevel Parallel Object-Oriented Framework for Design Optimization, Parameter Estimation, Uncertainty Quantification, and Sensitivity Analysis: Version 6.15 User's Manual." 11 2021. [Online]. Available: https://www.osti.gov/biblio/1829573

67. B. Adams, W. Bohnhoff, R. Canfield, W. Coomber, K. Dalbey, M. Ebeida, J. Eddy, M. Eldred, G. Geraci, R. Hooper, P. Hough, K. Hu, J. Jakeman, C. Kent, M. Khalil, K. Maupin, J. Monschke, E. Ridgway, A. Rushdi, D. Seidl, J. Stephens, L. Swiler, A. Tran, D. Vigil, T. Wildey, J. Winokur, F. Menhorn, and X. Zeng, "Dakota, A Multilevel Parallel Object-Oriented Framework for Design Optimization, Parameter Estimation, Uncertainty Quantification, and Sensitivity Analysis: Version 6.15 Reference Manual." 11 2021. [Online]. Available: https://www.osti.gov/biblio/1829573

68. H. Beer and F. Käppeler, "Neutron capture cross sections on Ba 138, Ce 1 4 0, 1 4 2, Lu 1 7 5, 1 7 6, and Ta 181 at 30 keV: Prerequisite for investigation of the Lu 176 cosmic clock," *Physical Review C*, vol. 21, no. 2, p. 534, 1980.

69. G. Feinberg, M. Friedman, A. Krása, A. Shor, Y. Eisen, D. Berkovits, D. Cohen, G. Giorginis, T. Hirsh, M. Paul *et al.*, "Quasi-stellar neutrons from the 7 li (p, n) 7 be reaction with an energy-broadened proton beam," *Physical Review C*, vol. 85, no. 5, p. 055810, 2012.

70. W. Ratynski and F. Käppeler, "Neutron capture cross section of Au 197: A standard for stellar nucleosynthesis," *Physical Review C*, vol. 37, no. 2, p. 595, 1988.

71. S. Mashnik, M. Chadwick, H. Hughes, R. Little, R. MacFarlane, L. Waters, and P. Young, "7-Li (p, n) nuclear data library for incident proton energies to 150 MeV," *arXiv preprint nucl-th/0011066*, 2000.

72. M. Drosg, "Sources of variable energy monoenergetic neutrons for fusion-related applications," *Nuclear Science and Engineering*, vol. 106, no. 3, pp. 279–295, 1990.

73. J. Meadows and D. Smith, "NEUTRONS FROM PROTON BOMBARDMENT OF NATURAL LITHIUM." Argonne National Lab., Ill., Tech. Rep., 1972.

74. N. Soppera, M. Bossant, and E. Dupont, "JANIS 4: an improved version of the NEA java-based nuclear data information system," *Nuclear Data Sheets*, vol. 120, pp. 294–296, 2014.

75. S. Kwon, C. Konno, M. Ohta, and S. Sato, "Problems on neutron production data of Be-9 in TENDL-2017 and-2019 deuteron sub-libraries," *Annals of Nuclear Energy*, vol. 169, p. 108932, 2022.

76. D. Smith, J. Meadows, and P. Guenther, "Investigation of thick-target neutron emission from Be-9 (d, n) B-10 AT Ed= 7 MeV for angles other than zero degrees," *Radiation Effects*, vol. 95, no. 1-4, pp. 285–289, 1986.

77. F. B. Brown, J. E. Sweezy, and R. Hayes, "Monte Carlo parameter studies and uncertainty analyses with MCNP5," Los Alamos National Lab.(LANL), Los Alamos, NM (United States), Tech. Rep., 2004.

REPORT DOCUMENTATION PAGE

Form Approved
OMB No. 0704–0188

1. REPORT DATE *(DD–MM–YYYY)*	2. REPORT TYPE	3. DATES COVERED *(From — To)*
24–03–2022	Master's Thesis	October 2020 - March 2022

4. TITLE AND SUBTITLE

Optimization of a Multi-Layered Target for a Pulsed Power Neutron Source

5a. CONTRACT NUMBER

5b. GRANT NUMBER

5c. PROGRAM ELEMENT NUMBER

6. AUTHOR(S)

Bretz, Zachary D., Civilian

5d. PROJECT NUMBER

5e. TASK NUMBER

5f. WORK UNIT NUMBER

7. PERFORMING ORGANIZATION NAME(S) AND ADDRESS(ES)

Air Force Institute of Technology
Graduate School of Engineering and Management (AFIT/EN)
2950 Hobson Way
WPAFB OH 45433-7765

8. PERFORMING ORGANIZATION REPORT NUMBER

AFIT-ENP-MS-22-M-080

9. SPONSORING / MONITORING AGENCY NAME(S) AND ADDRESS(ES)

Air Force Nuclear Weapons Center (AFNWC/ST)
2000 Wyoming Blvd SE
Albuquerque, NM 87123
POC: Col Clark Allred
clark.allred@us.af.mil / 505-321-1970

10. SPONSOR/MONITOR'S ACRONYM(S)

11. SPONSOR/MONITOR'S REPORT NUMBER(S)

12. DISTRIBUTION / AVAILABILITY STATEMENT

Distribution Statement A. Approved for public release; Distribution Unlimited.

13. SUPPLEMENTARY NOTES

This material is declared work of the U.S. Government and is not subject to copyright protection in the United States.

14. ABSTRACT

The ability to create neutron environments is critical fora wide variety of applications including national security, materials science, and medical research. It is also helpful in medical, material, and other research. The U.S. Naval Research Laboratory (NRL), Washington, DC, is interested in leveraging their pulsed-power facilities to produce an in-house, relatively inexpensive neutron source. NRL's facilities produce 2 MeV (from Gamble II) and 5 MeV (from Mercury) protons and deuterons. This research explored combinations of target materials to produce the most neutrons in the forward direction. Models of the reactions involved were first validated against literature experiments, then target designs were optimized with Dakota, a robust software suite used for various aspects of design exploration. The nuclear reactions and targets were modeled with MCNP, a Monte Carlo neutral particle transport code. A code base for scaling and future design work was also developed. The materials used in the optimization were lithium, beryllium, carbon, and deuterated polyethylene (CD_2).
The validation revealed discrepancies between the cross section libraries and literature. The CP2020 and JENDL/DEU libraries performed relatively well. The TENDL-2019 library greatly underperformed for the deuteron reactions. The ENDF/B-VIII.0 library also deviated in some cases from the existing data.
The optimizations resulted in four unique targets, but came with a large amount of uncertainty. Lithium was shown to be the better target for the proton reactions, while beryllium was better for deuteron reactions. There were some variations of beryllium-lithium combination targets that produced the most neutrons, but these need further investigation. The carbon and CD_2 were found to produce neutrons at a much lower rate than beryllium or lithium and were not used in any target.

15. SUBJECT TERMS

Neutron, Proton, Deuteron, Pulsed Power, Target, Neutron Target, Neutron Source, Multi-layered Target, Cross Sections, Cross Section Libraries, Monte Carlo, MCNP, MCNP6.2, Dakota, Optimization, Neutron Environments

16. SECURITY CLASSIFICATION OF:			17. LIMITATION OF ABSTRACT	18. NUMBER OF PAGES	19a. NAME OF RESPONSIBLE PERSON
a. REPORT	b. ABSTRACT	c. THIS PAGE			Manfredi, Juan J., AFIT/ENP
U	U	U	UU	110	19b. TELEPHONE NUMBER *(include area code)* (937) 255-6565 x4524; Juan.Manfredi@afit.edu